

Determining the parameters of the Minimal Supergravity Model from $2l + E_T^{miss} + (jets)$ final states at LHC.

D. Denegri¹, W.Majerotto², and L. Rurua^{2,3}

¹*Centre d'Etudes Nucléaire de Saclay, Gif-sur-Yvette, France*

²*Institut für Hochenergiephysik, Österreichische Akademie d. Wissenschaften, Vienna, Austria*

³*Institute of Physics, Tbilisi, Georgia*

Abstract

We analyse the events with two same-flavour, opposite-sign leptons + E_T^{miss} + (jets) as expected in pp collisions at LHC within the framework of the minimal Supergravity Model. The objective is the determination of the parameters m_0 and $m_{1/2}$ of this model (for a given value of $\tan\beta$). The signature $l^+l^- + E_T^{miss} + (jets)$ selects the leptonic decays of $\tilde{\chi}_2^0, \tilde{\chi}_2^0 \rightarrow \tilde{\chi}_1^0 l^+ l^-, \tilde{\chi}_2^0 \rightarrow \tilde{l}_{L,R}^\pm l^\mp \rightarrow \tilde{\chi}_1^0 l^+ l^-$. We exploit the fact that the invariant dilepton mass distribution has a pronounced structure with a sharp edge at the kinematical endpoint even in such an inclusive final state over a significant part of parameter space. We determine the domain of parameter space where the edge is expected to be visible. We show that a measurement of this edge already constrains the model parameters essentially to three lines in the $(m_0, m_{1/2})$ parameter plane. We work out a strategy to discriminate between the three-body leptonic decays of $\tilde{\chi}_2^0$ and the decays into sleptons $\tilde{l}_{L,R}$. This procedure may make it possible to get information on SUSY particle masses already with low luminosity, $L_{int} = 10^3 \text{ pb}^{-1}$.

1 Introduction

If 'low-energy' supersymmetry (SUSY) is realised in Nature it should show up at the Large Hadron Collider (LHC). Strongly interacting particles as gluinos and squarks will be most likely the first SUSY particles to be seen at LHC. Gluinos of mass less than ~ 2 TeV and squarks of mass less than ~ 1.5 TeV [1-3] can be detected, covering in such a way the whole theoretically motivated parameter space. LHC is also a good laboratory for the search of electro-weakly interacting particles, e.g. sleptons [4,5]. In a recent paper [6] it was shown within the minimal supergravity (mSUGRA) [7] model that sleptons in the mass range of ~ 100 to 400 GeV can be detected at LHC by investigating the signature *two leptons + E_T^{miss} + no jets*. However, this final state where direct production (Drell-Yan) of sleptons predominates requires high luminosity, $L_{int} = 10^5 \text{ pb}^{-1}$. Sleptons can be also produced indirectly in the decays of charginos and neutralinos, especially in $\tilde{\chi}_2^0 \rightarrow \tilde{l}_{L,R} l$ decays. The charginos and neutralinos, can in turn be produced directly or come from gluinos and/or squarks. This leads to final states with $\geq 2 \text{ leptons} + E_T^{miss} + (\text{jets})$. Actually, this indirect slepton production through \tilde{g}, \tilde{q} decays has the largest cross-section in a sizable region of the parameter space accessible at LHC and could allow sleptons to be already revealed at $L_{int} = 10^3 \text{ pb}^{-1}$, i.e. simultaneously with strongly interacting sparticles. Thus, indirect production of sleptons can be more important for observing a slepton signal than direct one [8]. Moreover, in such a way the mass reach for sleptons search can be extended up to $m_{\tilde{l}_L} \sim 740$ GeV.

Having evidence for SUSY at LHC, one of the next tasks will be to find out the underlying model and to determine the model parameters. In this paper we work out a method to determine SUSY parameters and suggest a strategy for getting information on masses of SUSY particles by means of the signature $l^+l^- + E_T^{miss} + (\text{jets})$. Our study is made within the framework of the minimal supergravity model (mSUGRA) [7]. In this model all scalar particles (sfermions and Higgs bosons) have a common mass m_0 at $M_{\text{GUT}} \approx 10^{16}$ GeV. The gaugino masses M_1, M_2, M_3 (corresponding to U(1), SU(2), and SU(3), respectively) unify to a common gaugino mass $m_{1/2}$, and all trilinear coupling parameters A_{ijk} have the same value A_0 at M_{GUT} . One also has unification of the electroweak and strong coupling parameters $\alpha_i, i = 1, 2, 3$ [9]. A further reduction of the parameters is given by invoking 'radiative symmetry breaking'. As a consequence, one has only the following input parameters: $m_0, m_{1/2}, A_0, \tan \beta, \text{sign}(\mu)$. Here $\tan \beta = \frac{v_2}{v_1}$, the ratio of the two vacuum expectation values of the two Higgs doublets, and μ is the Higgsino mass parameter. The whole SUSY particle spectrum can then be calculated by making use of renormalization group equations (RGE). This model is also incorporated in the Monte-Carlo generator ISASUSY [10] which is used in our analysis.

This paper is aimed at determining the parameters m_0 and $m_{1/2}$ with fixed $\tan \beta$. Knowing these parameters, we can calculate the masses of the superpartners using RGE. For this purpose, we study in detail the leptonic decays of $\tilde{\chi}_2^0$ which have some useful features. Within the mSUGRA model, $\tilde{\chi}_2^0$ has two-body decays, $\tilde{\chi}_2^0 \rightarrow \tilde{l}_{L,R}^\pm l^\mp$, in the region $m_0 \lesssim 0.5 \cdot m_{1/2}$ of the parameter space, whereas in the region $m_0 \gtrsim 0.5 \cdot m_{1/2}, m_{1/2} \lesssim 200$ GeV the $\tilde{\chi}_2^0$ has three-body decays, $\tilde{\chi}_2^0 \rightarrow l^+l^- \tilde{\chi}_1^0$. In both regions the invariant dilepton mass spectrum (M_{l+l^-}) has a maximum $M_{l+l^-}^{max}$, and therefore a pronounced structure with a sharp edge can be seen at the kinematical endpoint. This property was discussed first in ref. [11] in the case of three-body decays of $\tilde{\chi}_2^0$ and then in ref. [12] in the case of two-body decays. The generality of this feature, i.e. the observability of an edge in the

M_{l+l^-} spectrum even in inclusive $l^\pm l^\mp l^{+-}$ and $l^+ l^- + E_T^{miss}$ final states in a large part of the parameter space was shown in [13]. We will show how much the parameters are constrained by a measurement of the $M_{l+l^-}^{max}$ value of the dilepton mass spectra. Moreover, we will discuss a method, based on the analysis of the M_{l+l^-} spectrum, to find out whether the observed edge is due to the two-body or three-body decays of $\tilde{\chi}_2^0$.

2 Sparticle masses in mSUGRA

Within the Minimal Supersymmetric Standard Model (MSSM) the masses of the neutralinos are determined by the parameters M ($= m_{1/2}(M_Z)$), μ , and $\tan\beta$ using $M_1 \simeq \frac{5}{3}\tan^2\theta_W \simeq 0.5M$ (M_1 being the U(1) gaugino mass). In the following, we fix $\tan\beta = 2$ (we assume that $\tan\beta$ could be known from previous experiments) and take $A_0 = 0$. In mSUGRA $|\mu|$ quite generally turns out to be $|\mu| > M$, so that in this case $m(\tilde{\chi}_2^0) \simeq m(\tilde{\chi}_1^\pm) \simeq 2 \cdot m(\tilde{\chi}_1^0) \sim M$. Both $\tilde{\chi}_1^0$ and $\tilde{\chi}_2^0$ are gaugino like, $\tilde{\chi}_1^0$ is almost a pure $B - ino$, and $\tilde{\chi}_2^0$ almost a pure $W^3 - ino$. In supergravity the slepton masses are given by [14]:

$$m_{\tilde{l}_R}^2 = m_0^2 + 0.15m_{1/2}^2 - \sin^2\theta_W M_Z^2 \cos 2\beta \quad (1)$$

$$m_{\tilde{l}_L}^2 = m_0^2 + 0.52m_{1/2}^2 - 1/2(1 - 2\sin^2\theta_W)M_Z^2 \cos 2\beta \quad (2)$$

$$m_{\tilde{\nu}}^2 = m_0^2 + 0.52m_{1/2}^2 + 1/2M_Z^2 \cos 2\beta \quad (3)$$

Analogous equations exist for squarks [14]. Therefore, when the parameters m_0 , $m_{1/2}$ and $\tan\beta$ are known we can calculate all sparticle masses. A special case is the third generation of squarks and sleptons, where L-R mixing plays a crucial rôle.

3 Production and leptonic decay of $\tilde{\chi}_2^0$

Neutralinos $\tilde{\chi}_2^0$ can be produced at the LHC through a Drell-Yan mechanism (direct production), in association with strongly interacting sparticles, or in the decay chain of gluinos and squarks (indirect production). Gluino and squark pair production processes are the dominant source of $\tilde{\chi}_2^0$'s because of large strong interaction cross-sections. The branching ratios of gluino and squark decays into $\tilde{\chi}_2^0$ are also sizable and are shown in fig.1 as a function of the model parameters m_0 and $m_{1/2}$. One can see that the regions in $(m_0, m_{1/2})$ plane where the decays $\tilde{g} \rightarrow \tilde{\chi}_2^0 + X$ and $\tilde{q} \rightarrow \tilde{\chi}_2^0 + X$ are open, are complementary. In the region $m_0 \gtrsim 1.47 \cdot m_{1/2}$ gluinos are lighter than squarks and can decay into $\tilde{\chi}_2^0$, while squarks prefer to decay into gluinos. In the region $m_0 \lesssim 1.47 \cdot m_{1/2}$ squarks are lighter than gluinos and can decay into $\tilde{\chi}_2^0$, but gluinos decay into squarks. Hence the decays $\tilde{g} \rightarrow \tilde{\chi}_2^0 + X$ ($\tilde{q} \rightarrow \tilde{\chi}_2^0 + X$) and $\tilde{q} \rightarrow \tilde{g} \rightarrow \tilde{\chi}_2^0 + X$ ($\tilde{g} \rightarrow \tilde{q} \rightarrow \tilde{\chi}_2^0 + X$) can coexist (see also fig.1). Fig.2(a,b) shows $\sigma \times Br$ for indirect $\tilde{\chi}_2^0$ production from gluinos and squarks as a function of m_0 and $m_{1/2}$.

There are three different leptonic decays of $\tilde{\chi}_2^0$ interesting for our study: $\tilde{\chi}_2^0 \rightarrow l^+ l^- \tilde{\chi}_1^0$, $\tilde{\chi}_2^0 \rightarrow \tilde{l}_R^\pm l^\mp$ and $\tilde{\chi}_2^0 \rightarrow \tilde{l}_L^\pm l^\mp$. When decays of $\tilde{\chi}_2^0$ to sleptons are allowed, sleptons decay directly into the lightest supersymmetric particle ($lsp \equiv \tilde{\chi}_1^0$) with $Br(\tilde{l}_{L,R}^\pm \rightarrow \tilde{\chi}_1^0 l^\pm) = 100\%$.

Branching ratios of $\tilde{\chi}_2^0$ decays into leptons directly and via sleptons are shown in fig.3 as a function of m_0 and $m_{1/2}$. The regions where these decays are kinematically allowed are complementary in the parameter plane, depending on whether $\tilde{\chi}_2^0$ is lighter or heavier than $\tilde{l}_{L,R}$. Thus, one can distinguish three domains in the $(m_0, m_{1/2})$ plane, which are (also see fig.4):

$$\text{domain I } (m_0 \gtrsim 0.5 \cdot m_{1/2}, m_{1/2} \lesssim 200 \text{ GeV}) : \quad m_{\tilde{\chi}_2^0} < m_{\tilde{l}_{L,R}} \quad , \quad \text{with } \tilde{\chi}_2^0 \rightarrow \tilde{\chi}_1^0 ll$$

$$\text{domain II } (0.45 \cdot m_{1/2} \lesssim m_0 \lesssim 0.5 \cdot m_{1/2}) : \quad m_{\tilde{l}_R} < m_{\tilde{\chi}_2^0} < m_{\tilde{l}_L} \quad , \quad \text{with } \tilde{\chi}_2^0 \rightarrow \tilde{l}_R l$$

$$\text{domain III } (m_0 \lesssim 0.45 \cdot m_{1/2}) : \quad m_{\tilde{\chi}_2^0} > m_{\tilde{l}_L} \quad , \quad \text{with } \tilde{\chi}_2^0 \rightarrow \tilde{l}_L l$$

In domain III, the decay $\tilde{\chi}_2^0 \rightarrow \tilde{l}_R l$ would also be kinematically allowed, but since the $B - ino$ component of $\tilde{\chi}_2^0$ is very small, the coupling to $\tilde{l}_R l$ is also small. Therefore, the decay $\tilde{\chi}_2^0 \rightarrow \tilde{l}_R l$ is very much suppressed in the whole domain.

In fig.5 we show the regions for $\sigma \times Br(\tilde{\chi}_2^0 \rightarrow \tilde{\chi}_1^0 l^+ l^-) \sim 1$ and 0.1 pb, $\sigma \times Br(\tilde{\chi}_2^0 \rightarrow \tilde{l}_R^\pm l^\mp \rightarrow \tilde{\chi}_1^0 l^+ l^-) \sim 1$, 0.1 pb and $\sigma \times Br(\tilde{\chi}_2^0 \rightarrow \tilde{l}_L^\pm l^\mp \rightarrow \tilde{\chi}_1^0 l^+ l^-) \sim 1$, 0.002 pb in the $(m_0, m_{1/2})$ plane from indirect and associated $\tilde{\chi}_2^0$ production followed by decays to $\tilde{\chi}_1^0 l^+ l^-$ final states directly or via sleptons. One can see that there are regions in domains II and III where the mentioned decays coexist. Finally, in fig.6 we show $\sigma \times Br$ for indirect and associated production of $\tilde{\chi}_2^0$ decaying into leptons directly or via sleptons.

4 Determination of m_0 , $m_{1/2}$ and sparticle masses

In order to determine the parameters m_0 and $m_{1/2}$ we will exploit in the following the kinematical features of the two- and three-body leptonic decays of $\tilde{\chi}_2^0$.

As pointed out in [11], the decay $\tilde{\chi}_2^0 \rightarrow l^+ l^- \tilde{\chi}_1^0$ (domain I) has the useful kinematical property that the invariant mass of the two leptons M_{l+l^-} has a maximum at

$$M_{l+l^-}^{max} = m_{\tilde{\chi}_2^0} - m_{\tilde{\chi}_1^0}, \quad (4)$$

whereas for the decays $\tilde{\chi}_2^0 \rightarrow \tilde{l}_{L,R}^\pm l^\mp \rightarrow l^+ l^- \tilde{\chi}_1^0$ (domain II and III) the maximum of M_{l+l^-} is given by [12]:

$$M_{l+l^-}^{max} = \frac{\sqrt{(m_{\tilde{\chi}_2^0}^2 - m_{\tilde{l}}^2)(m_{\tilde{l}}^2 - m_{\tilde{\chi}_1^0}^2)}}{m_{\tilde{l}}}. \quad (5)$$

Thus, the M_{l+l^-} distribution has a very characteristic shape with a sharp edge at the kinematical endpoint $M_{l+l^-}^{max}$.

As the main source of $\tilde{\chi}_2^0$'s is their indirect production in gluino and squark decays, the most suitable signature for selecting the $\tilde{\chi}_2^0$ decays is provided by the topology with two same-flavour opposite-sign leptons accompanied by large missing transverse energy and usually accompanied by a high multiplicity of jets. In this paper we thus concentrate on the *two same-flavour, opposite-sign leptons + E_T^{miss} + (jets)* channel, where the final state leptons are electrons and muons.

4.1 CMS detector simulation

The simulations are done at the particle level, with parametrised detector responses based on detailed detector simulations. These parametrisations are adequate for the level of detector properties we want to investigate, and are the only practical ones in view of the multiplicity and complexity of the final state signal and background channels investigated. The essential ingredients for the investigation of SUSY channels are the response to jets, E_T^{miss} , the lepton identification and isolation capabilities of the detector, and the capability to tag b-jets.

The CMS detector simulation program CMSJET 3.2 [15] is used. It incorporates the full electro-magnetic (ECAL) and hadronic (HCAL) calorimeter granularity, and includes main calorimeter system cracks in rapidity and azimuth. The energy resolutions for muons, electrons (photons), hadrons and jets are parametrised. Transverse and longitudinal shower profiles are also included through appropriate parametrisations. The main detector features incorporated in the Monte-Carlo description are:

- Hadronic tracks, muons and electrons are measured up to $|\eta|=2.4$
- Deflection of charged particles due to the 4 T magnetic field is included.
- The resolution for the muon system is parametrised according to [16].
- The calorimetric coverage goes up to at $|\eta|=5$ for the HCAL and $|\eta|=2.6$ for the ECAL.

- ECAL energy resolution parametrized as:

$$\Delta E/E = 5\%/\sqrt{E} \oplus 0.5\%$$

- HCAL energy resolution is parametrised according to [17] as a function of η ; a typical hadron resolution is:

$$\Delta E/E = 80\%/\sqrt{E} \oplus 7\%$$

- Energy resolution for very forward calorimeter (VFCAL), in the parallel plate chambers option:

$$\Delta E/E = 90\%/\sqrt{E} \oplus 3\%$$

- Granularity of calorimeters:

| | $\eta - range$ | $\Delta\varphi \times \Delta\eta$ |
|--------------|------------------------|-----------------------------------|
| ECAL(barrel) | $ \eta < 1.57$ | 0.015x0.015 |
| | $1.57 < \eta < 1.65$ | crack |
| ECAL(endcap) | $1.65 < \eta < 2$ | 0.022x0.022 |
| | $2. < \eta < 2.35$ | 0.029x0.029 |
| | $2.35 < \eta < 2.61$ | 0.043x0.043 |
| HCAL | $ \eta < 2.26$ | 0.087x0.087 |
| | $2.26 < \eta < 2.6$ | 0.174x0.175 |
| | $2.6 < \eta < 3$ | 0.195x0.349 |
| VFCAL | $3 < \eta < 4$ | 10x10 cm^2 |
| | $4 < \eta < 5$ | 5x5 cm^2 |

- $E_{threshold}$ on cells:

- ECAL: $E_{threshold} = 50$ MeV

- HCAL: $E_{threshold} = 250$ MeV
- VFCAL: $E_{threshold} = 500$ MeV

- a modified UA1- jet finding algorithm with a cone size of $\Delta R=0.9$ (for description see CMSJET 3.5 [15]) is used for jet reconstruction.

4.2 Observability of edges in invariant dilepton mass distributions

In this chapter we determine the regions in the $(m_0, m_{1/2})$ parameter plane, where the characteristic edge in the M_{l+l^-} distribution can be observed in inclusive final states with *two same-flavour, opposite-sign leptons* + E_T^{miss} + (*jets*) with different luminosities at LHC.

Standard Model background processes are generated with PYTHIA 5.7 [18]. We use CTEQ2L structure functions. The largest background is due to $t\bar{t}$ production, with both W 's decaying into leptons, or one of the leptons from a W decay and the other from the b -decay of the same t -quark. We also considered other SM backgrounds: $W + jets$, WW , WZ , $b\bar{b}$ and $\tau\tau$ -pair production, with decays into electrons and muons. Chargino pair production $\tilde{\chi}_1^\pm \tilde{\chi}_1^\mp$ is the largest SUSY background but gives a small contribution compared to the signal.

To observe an edge in the M_{l+l^-} distributions with the statistics provided by an integrated luminosity $L_{int} = 10^3 \text{ pb}^{-1}$ in a significant part of the $(m_0, m_{1/2})$ parameter plane, it is enough to require two hard isolated leptons ($p_T^{l_{1,2}} > 15$ GeV) accompanied by large missing energy, $E_T^{miss} > 100$ GeV. Our criterion for observing an edge in the M_{l+l^-} distribution contains two requirements: $(N_{EV} - N_B)/\sqrt{N_{EV}} \gtrsim 5$ and $(N_{EV} - N_B)/N_B \gtrsim 1.3$, where N_{EV} is the number of events with $M_{l+l^-} \leq M_{l+l^-}^{max}$, and N_B is number of the expected background events. Fig.7 shows the invariant mass spectra of the two leptons at various $(m_0, m_{1/2})$ points from domains I, II and III, respectively. The observability of the "edge" varies from 77σ and signal to background ratio 31 at point (200,160) to 27σ and a signal to background ratio 2.3 at point (60,230). The appearance of the edges in the distributions is sufficiently pronounced already with $L_{int} = 10^3 \text{ pb}^{-1}$ in a significant part of $(m_0, m_{1/2})$ parameter plane, see fig.9. The edge position can be measured with a precision of ~ 0.5 GeV.

With increasing m_0 and $m_{1/2}$ cross-sections are decreasing, therefore higher luminosity and harder cuts are needed. To achieve maximal reach in $m_{1/2}$ with $L_{int} = 10^4 \text{ pb}^{-1}$ for points from domain III, a cut up to $E_T^{miss} > 300$ GeV is necessary to suppress the background sufficiently. For points with large m_0 (domain I) the transverse momentum p_T of the leptons and E_T^{miss} are not very large, but there are more hard jets due to gluino and squark decays. Thus for these points we keep the same cuts for leptons and missing energy as before ($p_T^{l_{1,2}} > 15$ GeV, $E_T^{miss} > 100$ GeV) and require in addition a jet multiplicity $N_{jet} \geq 3$, with energy $E_T^{jet} > 100$ GeV, in the rapidity range $|\eta_{jet}| < 3.5$. To optimise the edge visibility we also apply an azimuthal angle cut, $\Delta\phi(l^+l^-) < 120^\circ$. For points from domain II, the jet multiplicity requirement is also helpful. Right sleptons are too light to provide large lepton p_T and E_T^{miss} , and to use cuts on p_T^l and E_T^{miss} alone is not very advantageous. With $L_{int} = 10^5 \text{ pb}^{-1}$, to suppress the background at larger accessible $m_0, m_{1/2}$ values, we have to require at least 2 or 3 jets, depending on the $m_0, m_{1/2}$ region

to be explored. Fig.8 shows invariant dilepton mass distributions at some $(m_0, m_{1/2})$ points close to maximum reach with $L_{int} = 10^4 pb^{-1}$ and $L_{int} = 10^5 pb^{-1}$ respectively.

The regions of the $(m_0, m_{1/2})$ parameter plane where an edge in the M_{l+l^-} spectra can be observed at different luminosities are shown in fig.9. In fig.10 we show separately the three domains where an edge due to $\tilde{\chi}_2^0 \rightarrow ll\tilde{\chi}_1^0$, $\tilde{l}_R l$ and $\tilde{l}_L l$ decays can be observed at $L_{int} = 10^3 pb^{-1}$. One can notice a small overlapping region, where we expect to observe two edges, due to $\tilde{\chi}_2^0 \rightarrow l^+l^-\tilde{\chi}_1^0$ and to $\tilde{\chi}_2^0 \rightarrow \tilde{l}_R^\pm l^\mp \rightarrow l^+l^-\tilde{\chi}_1^0$ decays (*case 1*). With increasing luminosity and correspondingly higher statistics, this overlapping region increases, see figs.11 and 12. These plots show the same as fig.10, but for $L_{int} = 10^4 pb^{-1}$ and $L_{int} = 10^5 pb^{-1}$, respectively. An additional region appears where two edges can be observed simultaneously, due to $\tilde{\chi}_2^0 \rightarrow \tilde{l}_R^\pm l^\mp \rightarrow l^+l^-\tilde{\chi}_1^0$ and $\tilde{\chi}_2^0 \rightarrow \tilde{l}_L^\pm l^\mp \rightarrow l^+l^-\tilde{\chi}_1^0$ decays (*case 2*). These regions (*case 1* and *2*) are due to the coexistence of different $\tilde{\chi}_2^0$ decay modes has been seen in fig.5. An example of a M_{l+l^-} distribution for *case 1* is shown in fig.13.

Therefore, to a given integrated luminosity at LHC ($L_{int} = 10^3 pb^{-1}$ to $10^5 pb^{-1}$) there corresponds a definite parameter region where the characteristic structure in the M_{l+l^-} distribution can be seen. This fact already gives a preliminary information about the parameters m_0 and $m_{1/2}$. The observation of two edges would give even stronger constraints.

4.3 $M_{l+l^-}^{max}$ analysis of $(m_0, m_{1/2})$ parameter plane

Within mSUGRA all sparticle masses for every point $(m_0, m_{1/2})$ can be calculated. The expected edge position $M_{l+l^-}^{max}$ in the dilepton mass distribution can then be obtained from eqs.(4) and (5). In fig.14 we show contours for various expected values of $M_{l+l^-}^{max}$ in the $(m_0, m_{1/2})$ parameter plane. Different lines with the same value of $M_{l+l^-}^{max}$ belong to domains I, II and III (with the corresponding decay mode of $\tilde{\chi}_2^0$). The region of $M_{l+l^-}^{max}$ becoming accessible at LHC is:

$$\begin{array}{llll} \text{for} & \tilde{\chi}_2^0 \rightarrow \tilde{\chi}_1^0 l^+ l^- & - & 50 \text{ GeV} \lesssim M_{l+l^-}^{max} \lesssim 90 \text{ GeV} \\ & \tilde{\chi}_2^0 \rightarrow \tilde{l}_R l & - & M_{l+l^-}^{max} \gtrsim 10 \text{ GeV} \\ & \tilde{\chi}_2^0 \rightarrow \tilde{l}_L l & - & M_{l+l^-}^{max} \gtrsim 20 \text{ GeV} \end{array}$$

More specifically, at low luminosity, $L_{int} = 10^3 pb^{-1}$, at the beginning of the LHC operation, the accessible values of $M_{l+l^-}^{max}$ lie in the following ranges (see figs.10 and 14):

$$\begin{array}{llll} \text{for} & \tilde{\chi}_2^0 \rightarrow \tilde{\chi}_1^0 l^+ l^- & - & 50 \text{ GeV} \lesssim M_{l+l^-}^{max} \lesssim 80 \text{ GeV} \\ & \tilde{\chi}_2^0 \rightarrow \tilde{l}_R l & - & 10 \text{ GeV} \lesssim M_{l+l^-}^{max} \lesssim 110 \text{ GeV} \\ & \tilde{\chi}_2^0 \rightarrow \tilde{l}_L l & - & 20 \text{ GeV} \lesssim M_{l+l^-}^{max} \lesssim 120 \text{ GeV} \end{array}$$

It follows from the discussion above that a measurement of $M_{l+l^-}^{max}$ in the dilepton mass distribution, with a single edge, constrains the parameters in general to three lines in the

$(m_0, m_{1/2})$ parameter plane. In case of $M_{l^+l^-}^{max} \gtrsim 90$ GeV the constraint is stronger, there are just two possible lines. The most favourable case is when the measured $M_{l^+l^-}^{max}$ value is large, $M_{l^+l^-}^{max} \gtrsim 180$ GeV. Then one is left with a single line in the $(m_0, m_{1/2})$ parameter plane. For the present study we have chosen, as an example of the general situation, the case of $M_{l^+l^-}^{max} = 74 \pm 1$ GeV, with three lines corresponding to the domains I,II and III, respectively. The next step is to find out which line in the $(m_0, m_{1/2})$ plane is the right one. To this purpose we have analysed points along these lines, given in tables 1-3.

The study is made for the low luminosity case, $L_{int} = 10^3$ pb $^{-1}$.

Table 1. $M_{l^+l^-}^{max}$ values (in GeV) at the investigated $(m_0, m_{1/2})$ points from domain I, $\tilde{\chi}_2^0 \rightarrow \tilde{\chi}_1^0 + l^+ + l^-$.

| | (120,160) | (130,160) | (180,160) | (200,160) | (220,160) | (240,160) | (290,160) | (350,160) |
|--------------------|-----------|-----------|-----------|-----------|-----------|-----------|-----------|-----------|
| $M_{l^+l^-}^{max}$ | 74 | 74 | 74 | 74 | 74 | 74 | 74 | 73.7 |

Table 2. $M_{l^+l^-}^{max}$ values (in GeV) at the investigated $(m_0, m_{1/2})$ points from domain II, $\tilde{\chi}_2^0 \rightarrow \tilde{l}_R^\pm + l^\mp \rightarrow \tilde{\chi}_1^0 + l^+ + l^-$.

| $(m_0, m_{1/2}) \rightarrow$ | (80,162) | (90,170) | (105,180) | (110,187) | (120,195) |
|------------------------------|----------|----------|-----------|-----------|-----------|
| $M_{l^+l^-}^{max}$ | 74 | 74 | 73 | 75 | 73 |

Table 3. $M_{l^+l^-}^{max}$ values (in GeV) at the investigated $(m_0, m_{1/2})$ points from domain III, $\tilde{\chi}_2^0 \rightarrow \tilde{l}_L^\pm + l^\mp \rightarrow \tilde{\chi}_1^0 + l^+ + l^-$.

| $(m_0, m_{1/2}) \rightarrow$ | (20,195) | (40,210) | (60,230) | (80,255) |
|------------------------------|----------|----------|----------|----------|
| $M_{l^+l^-}^{max}$ | 73 | 73 | 73 | 73 |

One should first notice that the observation of two edges at $L_{int} = 10^3$ pb $^{-1}$ would determine the $(m_0, m_{1/2})$ point uniquely. This is due to the fact that the set of the edge position values in the $M_{l^+l^-}$ spectrum is different at each point of the parameter region (*case 1*), where two edges are expected to be observed at 10^3 pb $^{-1}$, see figs.10 and 14. With a luminosity $L_{int} = 10^4$ pb $^{-1}$ the positions of the two edges will fix two $(m_0, m_{1/2})$ points, belonging to domains II and III and corresponding to *case 1* and *case 2*, respectively. At high luminosity, $L_{int} = 10^5$ pb $^{-1}$, the observation of two edges can give up to three possible $(m_0, m_{1/2})$ points. One of them is from domain II, corresponding to *case 1*. The lines $M_{l^+l^-}^{max} = const$ corresponding to $\tilde{\chi}_2^0 \rightarrow \tilde{l}_R l$ decays have the form of an ellipse and can cross the $M_{l^+l^-}^{max} = const$ lines corresponding to $\tilde{\chi}_2^0 \rightarrow \tilde{l}_L l$ decays twice. Hence, two points with the same set of edge positions in the $M_{l^+l^-}$ spectrum can be found in domain III corresponding to *case 2*. A discrimination between these points is possible on basis of the event kinematics, and/or by an analysis of the total event rate and the relative number of events corresponding to the two peaks, (see figs.5,10-12).

4.4 Discrimination between different $\tilde{\chi}_2^0$ leptonic decays

For a definite value of the edge position $M_{l+l^-}^{max}$ one expects a different shape of the M_{l+l^-} -distributions in two- and three-body decays (see fig.13, where the first peak is due to a two-body decay of $\tilde{\chi}_2^0$ and the second one due to a three-body decay). As we have seen from figs.7 and 8 the signal events contribute in the interval $0 \lesssim M_{l+l^-} \lesssim M_{l+l^-}^{max}$. In the following we only consider events in this mass region. The average value $\langle M_{l+l^-} \rangle$ of signal and background events of this mass region is shown in fig.15 as a function of m_0 . The errors are calculated by taking into account the statistical error, a systematic error in the measurement of the edge position, and a systematic error of 30 % for background uncertainty (the main background is $t\bar{t}$). One clearly sees that $\langle M_{l+l^-} \rangle$ is significantly smaller in the case of a direct three-body decay $\tilde{\chi}_2^0 \rightarrow ll\tilde{\chi}_1^0$. Thus the shape of the dilepton mass spectrum already allows one to decide whether $\tilde{\chi}_2^0$ decays into a slepton or not.

In order to distinguish between domains II and III, we suggest to use the fact that in general the contour lines with the same $M_{l+l^-}^{max}$ for right and left sleptons have no overlap in $m_{1/2}$ in regions of parameter space which are accessible at a given luminosity, see figs.9 and 14 as an example. It means that the masses of $\tilde{\chi}_1^0$'s are different for these two lines, and hence E_T^{miss} is expected to be different. In fig.16 we show the $\langle E_T^{miss} \rangle$ values for events with $\tilde{\chi}_2^0 \rightarrow \tilde{l}_{L,R}^\pm l^\mp \rightarrow l^+l^- \tilde{\chi}_1^0$ decays after the cuts $p_T^{l_{1,2}} > 15$ GeV and $E_T^{miss} > 100$ GeV, $M_{l+l^-} < M_{l+l^-}^{max}$. The errors are calculated by taking into account the statistical error and a systematic error in the measurement of the edge position. As can be seen from fig.16, $\langle E_T^{miss} \rangle$ is larger in the case of $\tilde{\chi}_2^0 \rightarrow \tilde{l}_L^\pm l^\mp \rightarrow l^+l^- \tilde{\chi}_1^0$ than in the case of $\tilde{\chi}_2^0 \rightarrow \tilde{l}_R^\pm l^\mp \rightarrow l^+l^- \tilde{\chi}_1^0$ as expected.

4.4.1 Event rate analysis

When the correct $M_{l+l^-}^{max}$ line is chosen, the last step is to find the point $(m_0, m_{1/2})$ on this line. In general the cross section falls with increasing $m_{1/2}$ and m_0 . Thus, we study the event rate along the corresponding $M_{l+l^-}^{max}$ line. We first discuss the domain III, where the situation is simpler. For the event rate analysis at $L_{int} = 10^3$ pb $^{-1}$, to reduce the uncertainties due to background, we use a harder cut on E_T^{miss} , $E_T^{miss} > 130$ GeV. The dependence of the expected event rate on m_0 is shown in fig.17. The errors are calculated by taking into account the statistical error and a systematic error of 30 % for background uncertainty. A systematic error due to the precision of the edge position measurement is also taken into account. From the observed event rate we can then determine m_0 with a good accuracy, $\delta m_0 \simeq 4$ GeV. The parameter $m_{1/2}$ is then given by the $M_{l+l^-}^{max}$ -line in the $(m_0, m_{1/2})$ plane. The precision obtained in such a way is $\delta m_{1/2} \simeq 4$ GeV.

In domain II, the event rate along a line of definite $M_{l+l^-}^{max}$ is first increasing and then decreasing with m_0 , see fig.18. This is mainly due to the change in the branching ratios (see fig.4). The dependence of the event rate is, however, such that m_0 cannot be determined uniquely. To a given event rate there correspond in general two m_0 values. The ambiguity can, however, be solved at high luminosity $L_{int} = 10^5$ pb $^{-1}$, when two edges in the M_{l+l^-} distribution can be observed.

For domain I, the m_0 dependence of the event rate is shown in fig.19a, again for $M_{l+l^-}^{max} \simeq 74 \pm 1$ GeV. Notice the steep increase of the rate at $m_0 \simeq 120 - 130$ GeV. This is due to the fact that the decay channel $\tilde{\chi}_2^0 \rightarrow ll\tilde{\chi}_1^0$ is just opening in this region. As can be seen from the curve in fig.19a, there is an ambiguity in the determination of m_0 if the event rate is in the region $3700 \lesssim N_{EV} \lesssim 5600$ or 120 GeV $\lesssim m_0 \lesssim 240$ GeV. Here it

helps if we look at the average number of jets $\langle N_{jet} \rangle$ in the events under study. Fig.19b shows $\langle N_{jet} \rangle$ as a function of m_0 . $\langle N_{jet} \rangle$ is rising with m_0 as more jets are produced as the squarks become heavier. With the measured $\langle N_{jet} \rangle$ we can resolve the ambiguity in the mentioned region $120 \text{ GeV} \lesssim m_0 \lesssim 240 \text{ GeV}$ and thus determine m_0 with $\delta m_0 \simeq 7-3 \text{ GeV}$.

5 Conclusions

In this paper we have performed a detailed analysis of events with the signature $l^+l^- + E_T^{miss} + (jets)$ to be expected in pp collisions at LHC. Our aim has been to determine the parameters m_0 and $m_{1/2}$ of the Minimal Supergravity Model and to get information on the mass spectrum of SUSY particles, assuming knowledge of $\tan\beta$ from previous experiments. We have exploited the property of the $\tilde{\chi}_2^0$ leptonic decays $\tilde{\chi}_2^0 \rightarrow l^+l^-\tilde{\chi}_1^0$, $\tilde{\chi}_2^0 \rightarrow \tilde{l}_{L,R}l \rightarrow l^+l^-\tilde{\chi}_1^0$ that the invariant mass of the two final leptons has a maximum, $M_{l^+l^-}^{max}$, clearly visible even in inclusive production. We have determined for different luminosities the regions in the $(m_0, m_{1/2})$ parameter plane where one or two edges can be observed in the invariant dilepton mass distributions. These regions already give preliminary information about the model parameters. The appearance of the edges in the $M_{l^+l^-}$ distributions can be already seen with a luminosity $L_{int} = 10^3 \text{ pb}^{-1}$. Therefore we have concentrated on a low luminosity study. On the other hand, in case no such observation will be made at this luminosity, the corresponding parameter region can be excluded, and the same analysis can be done at higher luminosity.

We have shown that a measurement of the $M_{l^+l^-}^{max}$ value constrains the parameters mainly to three lines in the $(m_0, m_{1/2})$ parameter plane. The lines correspond to the decay modes $\tilde{\chi}_2^0 \rightarrow l^+l^-\tilde{\chi}_1^0$, $\tilde{l}_L l \rightarrow l^+l^-\tilde{\chi}_1^0$, $\tilde{l}_R l \rightarrow l^+l^-\tilde{\chi}_1^0$ respectively. We have worked out a method to discriminate the three-body from the two-body $\tilde{\chi}_2^0$ decays. In the case of three-body $\tilde{\chi}_2^0$ decays the parameter $m_{1/2}$ can be determined by the measured value of $M_{l^+l^-}^{max}$ with a precision of $\sim 0.5 \text{ GeV}$. The parameter m_0 can then be determined from the observed event rate with a precision of 7-3 GeV. In the case of two-body $\tilde{\chi}_2^0$ decays, a measurement of the missing transverse energy can allow one to distinguish between the two possible decays $\tilde{\chi}_2^0 \rightarrow \tilde{l}_L l$ and $\tilde{\chi}_2^0 \rightarrow \tilde{l}_R l$, but a more detailed study is needed. By an event rate analysis along the corresponding line in the $(m_0, m_{1/2})$ plane we can determine m_0 and $m_{1/2}$, $\delta m_0 \sim \delta m_{1/2} \sim 4 \text{ GeV}$.

Knowing m_0 , $m_{1/2}$ and $\tan\beta$, the masses of all SUSY particles (except for the 3rd generation of squarks and sleptons) are calculated by RGE. The precisions which can be achieved are $\sim 1-6 \text{ GeV}$.

In such a way it is possible to obtain information about SUSY particle masses already with low luminosity ($L = 10^3 \text{ pb}^{-1}$) even without having direct experimental evidence for their existence. This is especially important for sleptons in a parameter region where high luminosity would be necessary to detect them through direct production.

This study has been performed for $\tan\beta = 2$, but it is also possible for high values of $\tan\beta$. Most likely, for large $\tan\beta \gtrsim 30$ a higher luminosity will be needed because of smaller branching ratios of the $\tilde{\chi}_2^0$ leptonic decays.

Let us mention some further interesting aspects of this work. Selecting the two-body $\tilde{\chi}_2^0$ leptonic decays by our method represents an indirect evidence for sleptons in the framework of mSUGRA. In this way it is possible to probe slepton masses up to

~ 740 GeV well beyond what is possible in direct [5,6] searches. As it has been shown in this study, the edge in the invariant dilepton mass distributions is expected to appear at $M_{l+l^-}^{max} \gtrsim 10$ GeV, being quite generally a signal for a two- or three-body decay of some abundantly produced heavy object. Hence such an observation may serve as a first evidence for physics Beyond the Standard Model, and if observed with significant E_T^{miss} it would be a clear evidence for SUSY, more specifically for $\tilde{\chi}_2^0$ production.

Acknowledgements

We especially thank Howard Baer for answering many questions and for very useful discussions. We would like to thank Alfred Bartl for his interest in this work and valuable discussions. L.R. thanks for financial support by the Austrian Academy of Sciences.

References

- [1] Proc. of the ECFA Large Hadron Collider Workshop, Aachen, 1990, CERN 90-10, ECFA 90-133 (G. Jarlskog, P. Rein, etc.);
CMS Collaboration, Technical Proposal, LHCC/P2 (1994);
ATLAS Collaboration, Technical Proposal, LHCC/P2 (1994).
- [2] H. Baer, C-H. Chen, F. Paige and X. Tata, Phys. Rev. **D 52**, 2746 (1995); Phys. Rev. **D 53**, 6241 (1996);
I. Hinchliffe, J. Womersley, LBNL-38997.
- [3] S. Abdullin, CMS TN/96-095.
- [4] F. del Aguila and Ll. Ametller, Phys. Lett. **B 261**, 326 (1991).
- [5] H. Baer, C-H. Chen, F. Paige and X. Tata, Phys. Rev. **D 49**, 3283 (1994).
- [6] D. Denegri, L. Rurua, N. Stepanov, CMS TN/96-059.
- [7] For reviews, see H.P. Nilles, Phys. Rep. **110**, 1 (1984);
P. Nath, R. Arnowitt and A. Chamseddine, Applied N=1 Supergravity, ICTP series in Theoretical Physics (World Scientific, Singapore, 1984);
M. Drees and S.P. Martin, hep-ph/9504324.
- [8] L. Rurua, presentations to CMS Collaboration Meetings, January and July 1996, and in the LHCC SUSY Workshop, CERN, October 29-30, 1996, CMS Document 1996-149 (PH-SUSY);
D. Denegri, L. Rurua, N. Stepanov, CMS TN/96-059.
- [9] C. Giunti, C.W. Kim and U.W. Lee, Mod. Phys. Lett. **A 6**, (1991);
J. Ellis, S. Kelley and D.V. Nanopoulos, Phys. Lett. **B 260**, (1991) 161;
U. Amaldi, W. de Boer and H. Furstenau, Phys. Lett. **B 260**, 447 (1991);
P. Langacker and M. Luo, Phys. Rev. **D 44**, 817 (1991).

- [10] F. Paige and S. Protopopescu, in *Supercollider Physics*, p. 41, ed. D. Soper (World Scientific, 1986);
H. Baer, F. Paige, S. Protopopescu and X. Tata, in *Proceedings of the Workshop on Physics at Current Accelerators and Superolliders*, ed. J. Hewett, A. White and D. Zeppenfeld (Argonne National Laboratory, 1993).
- [11] H. Baer, K. Hagiwara, X. Tata, *Phys. Rev. D* **35**, 1598 (1987);
H. Baer, D.D. Karatas, X. Tata, *Phys. Rev. D* **42**, 2259 (1990) (fig. 6a);
H. Baer, C. Kao, X. Tata, *Phys. Rev. D* **48**, 5175 (1993);
H. Baer, C.-H. Chen, F. Paige, X. Tata, *Phys. Rev. D* **50**, 4508 (1994).
- [12] F. Paige, Determining SUSY particle masses at LHC, Proc. of the 1996 DPF/DPB Summer Study on High-Energy Physics "New Directions for High-Energy Physics", Snowmass, Colorado, 1996, p.710;
A.Bartl et al., Supersymmetry at LHC, *ibidem*, p.693;
J. Amundson et al., Report of the Supersymmetry Theory Subgroup, *ibidem*, p.655.
- [13] CMS presentation at the LHCC SUSY Workshop, CERN, October 29-30, 1996, CMS Document 1996-149 (PH-SUSY).
- [14] K. Inoue, A. Kakuto, H. Komatsu, and S. Takeshita, *Prog. Theor. Phys.* **68**, 927 (1982).
- [15] S. Abdullin, A. Khanov and N. Stepanov, CMS TN/94-180.
- [16] V. Karimaki, CMS TN/94-151.
- [17] V. Genchev, L. Litov, Study of the CMS TP calorimetry system, CMS TN/94-272 (1994).
- [18] T. Sjöstrand, *Comp. Phys. Com.* **39**, 347 (1986);
T. Sjöstrand and M. Bengtsson, *Comp. Phys. Com.* **43**, 367 (1987);
H.U. Bengtsson and T. Sjöstrand, *Comp. Phys. Com.* **46**, 43 (1987);
T. Sjöstrand, CERN-TH.7112/93.
- [19] H. Baer, M. Brhlik, *Phys. Rev. D* **53**, 597 (1996).

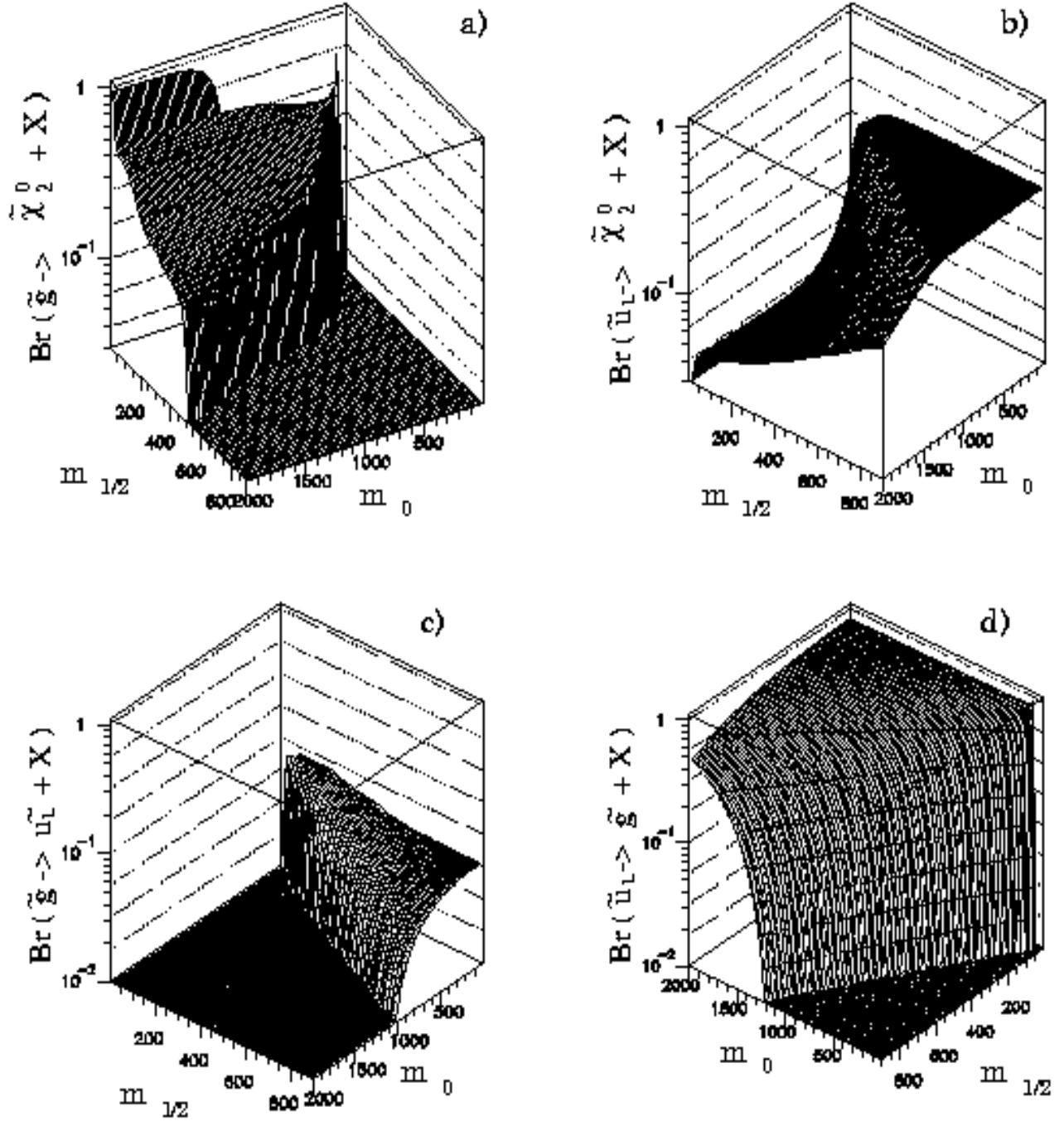


Figure 1: Decay branching ratios as a function of m_0 and $m_{1/2}$ (in GeV) for: a) $\tilde{g} \rightarrow \tilde{\chi}_2^0 + X$, b) $\tilde{u}_L \rightarrow \tilde{\chi}_2^0 + X$ and c) $\tilde{g} \rightarrow \tilde{u}_L + X$, d) $\tilde{u}_L \rightarrow \tilde{g} + X$, for $\tan\beta = 2$, $A_0 = 0$, $\mu < 0$.

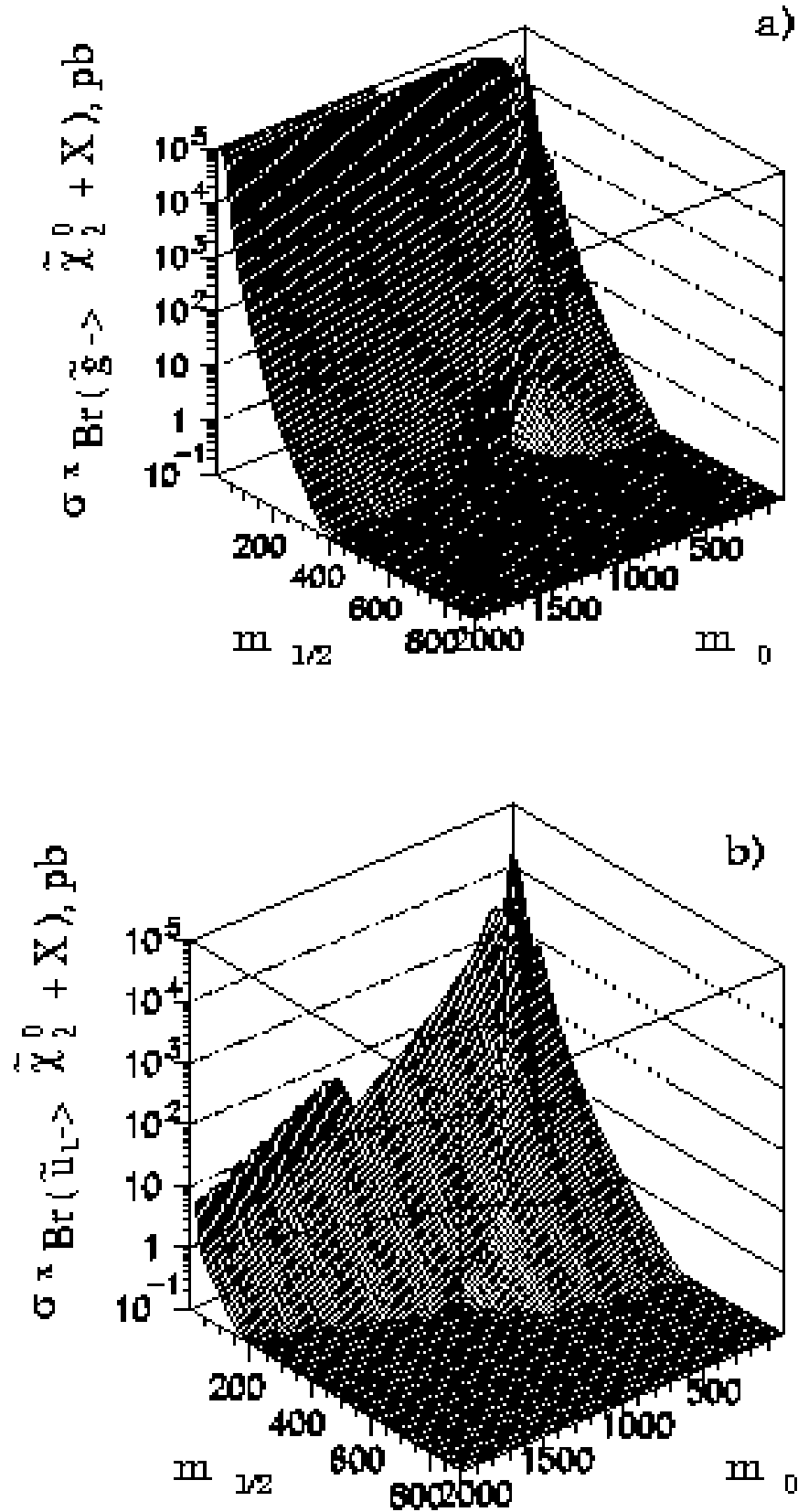


Figure 2: Sigma times branching ratios as a function of m_0 and $m_{1/2}$ (in GeV) for indirect $\tilde{\chi}_2^0$ production from gluinos (a) and squarks (b), for $\tan\beta = 2$, $A_0 = 0$, $\mu < 0$.

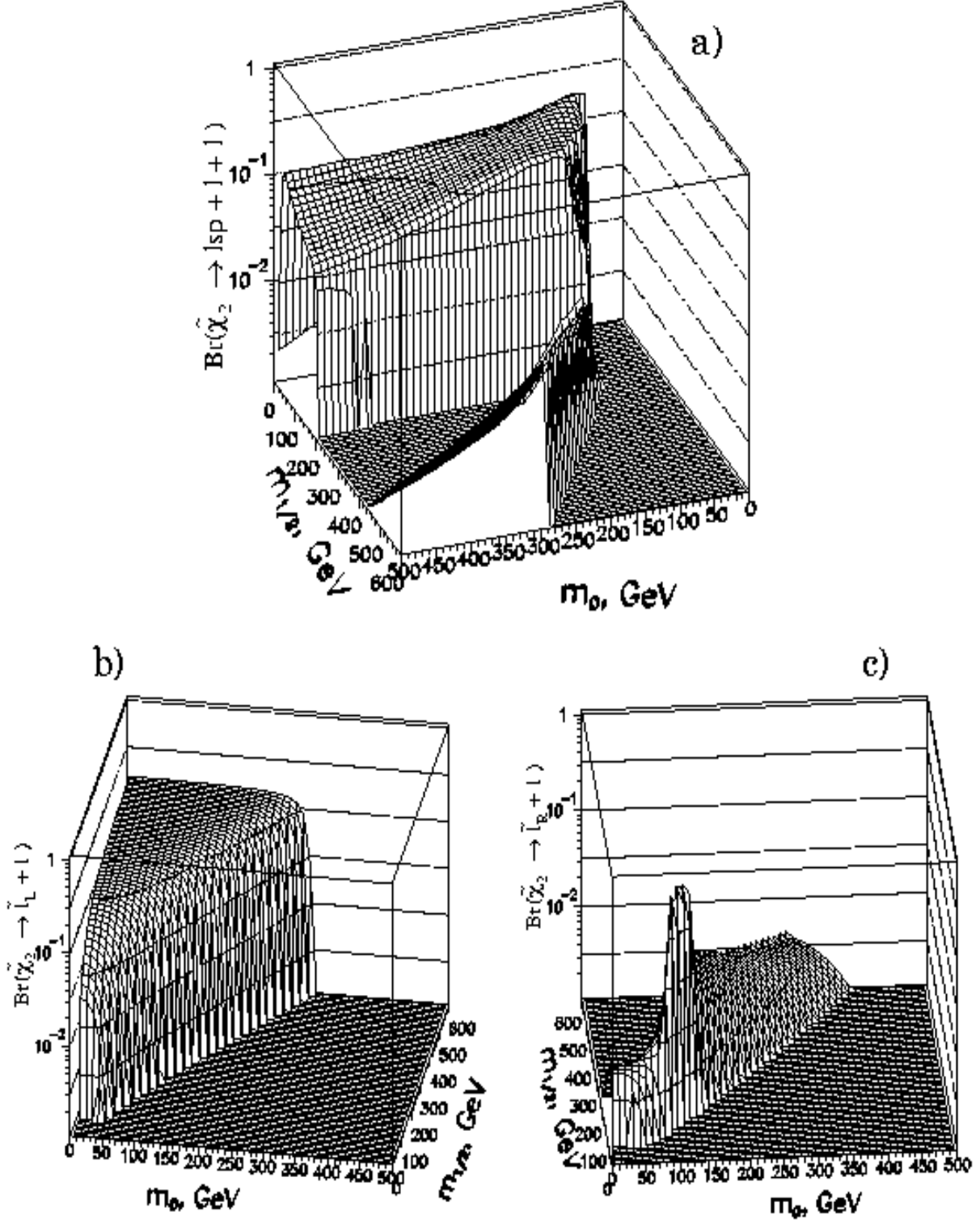


Figure 3: Branching ratios of $\tilde{\chi}_2^0$ decays: a) $\tilde{\chi}_2^0 \rightarrow \tilde{\chi}_1^0 l^+ l^-$, b) $\tilde{\chi}_2^0 \rightarrow \tilde{l}_L^\pm l^\mp$ and c) $\tilde{\chi}_2^0 \rightarrow \tilde{l}_R^\pm l^\mp$ as a function of m_0 and $m_{1/2}$, for $\tan \beta = 2$, $A_0 = 0$, $\mu < 0$.

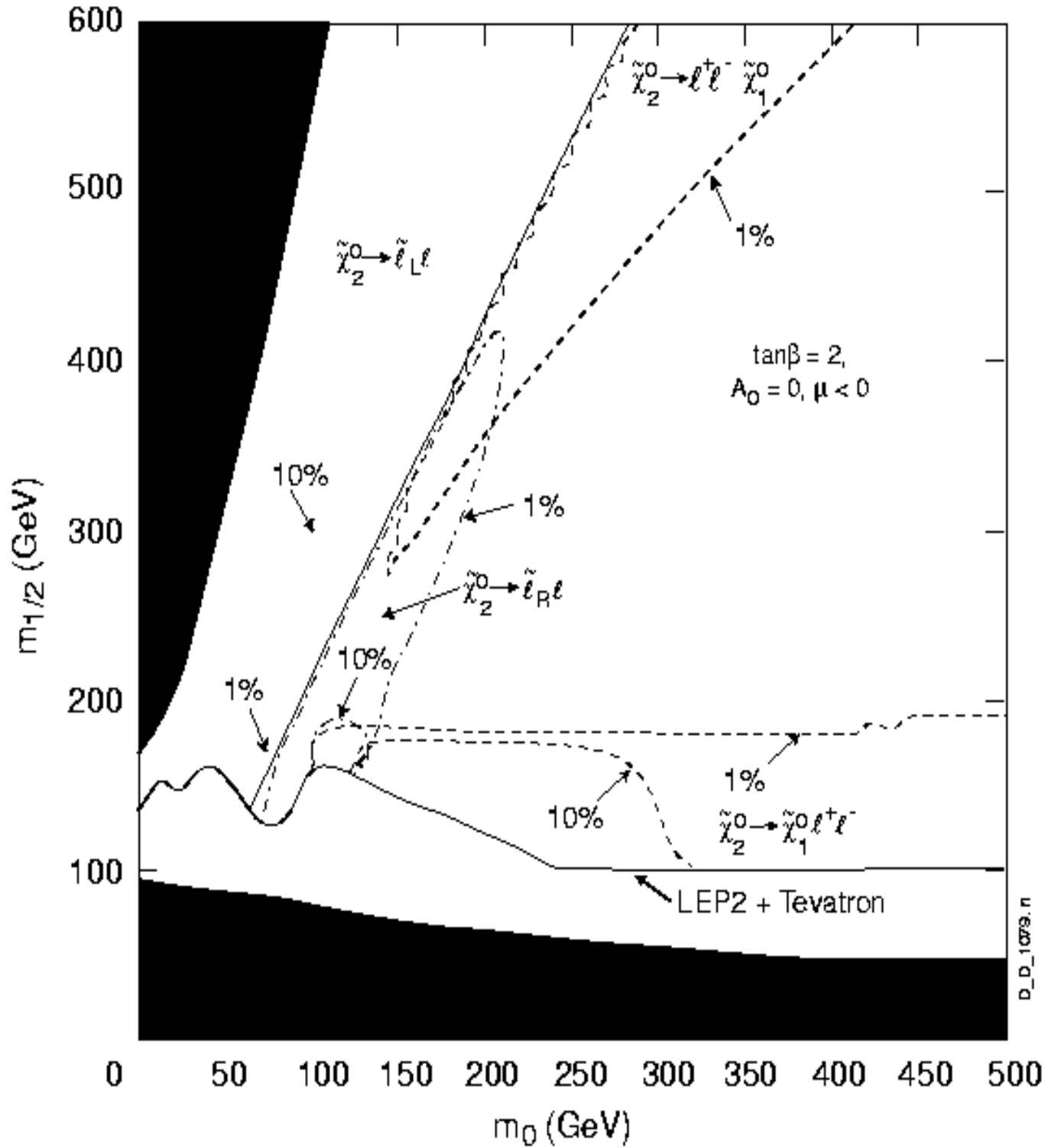


Figure 4: Domains of the decays $\tilde{\chi}_2^0 \rightarrow \tilde{\chi}_1^0 l^+ l^-$ (dashed line), $\tilde{\chi}_2^0 \rightarrow \tilde{l}_L^+ l^-$ (solid line) and $\tilde{\chi}_2^0 \rightarrow \tilde{l}_R^+ l^-$ (dashed-dotted line) in the $(m_0, m_{1/2})$ plane, corresponding to decay branching ratios in excess of 1% and 10% respectively, $\tan\beta = 2$, $A_0 = 0$, $\mu < 0$.

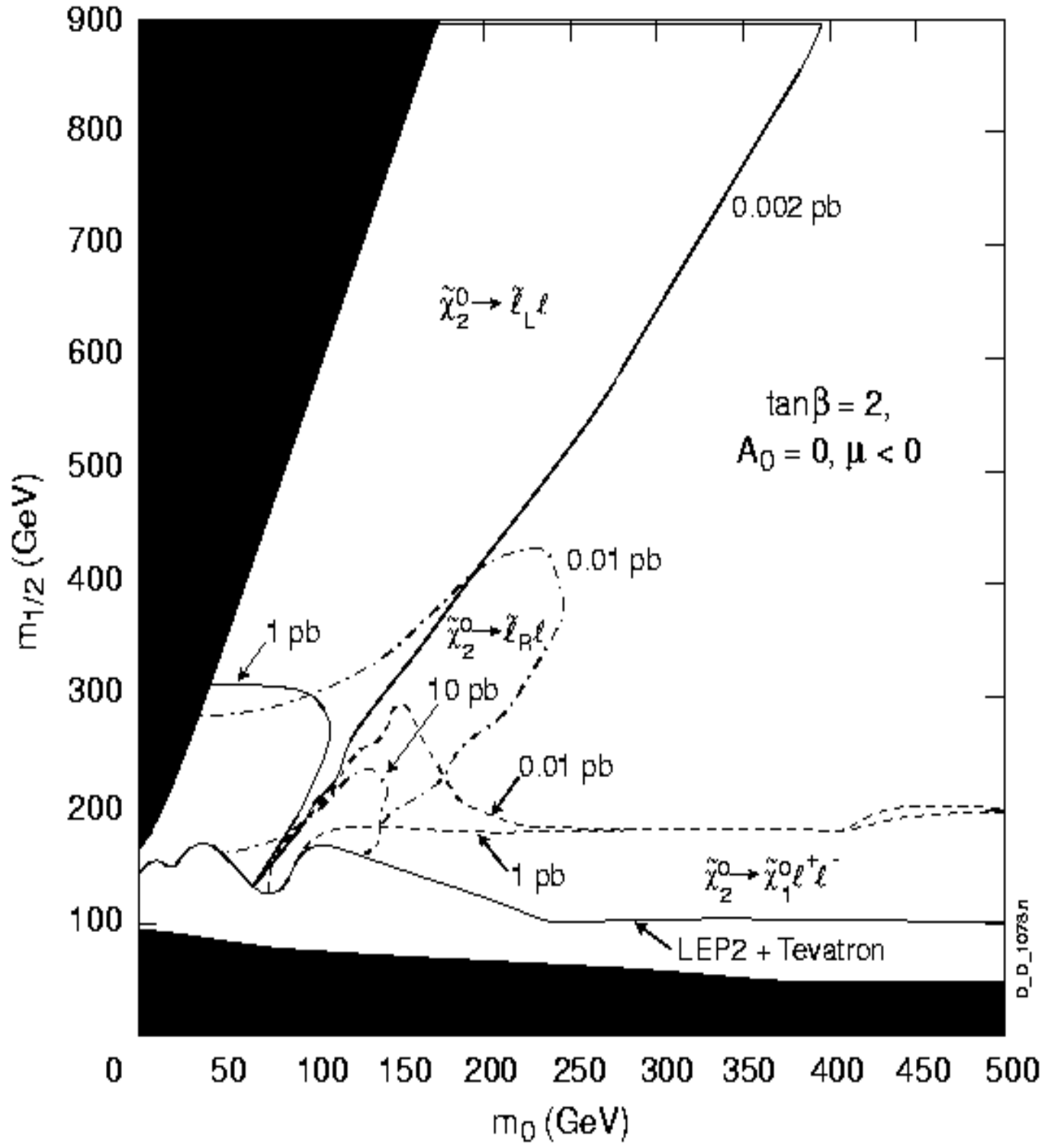


Figure 5: Contour lines for cross-section times branching ratios in the $(m_0, m_{1/2})$ plane for indirect and associated $\tilde{\chi}_2^0$ production followed by decays: $\tilde{\chi}_2^0 \rightarrow \tilde{\chi}_1^0 l^+ l^-$ (dashed line), $\tilde{\chi}_2^0 \rightarrow \tilde{l}_L^\pm l^\mp \rightarrow \tilde{\chi}_1^0 l^+ l^-$ (solid line) and $\tilde{\chi}_2^0 \rightarrow \tilde{l}_R^\pm l^\mp \rightarrow \tilde{\chi}_1^0 l^+ l^-$ (dashed-dotted line), $\tan\beta = 2$, $A_0 = 0$, $\mu < 0$.

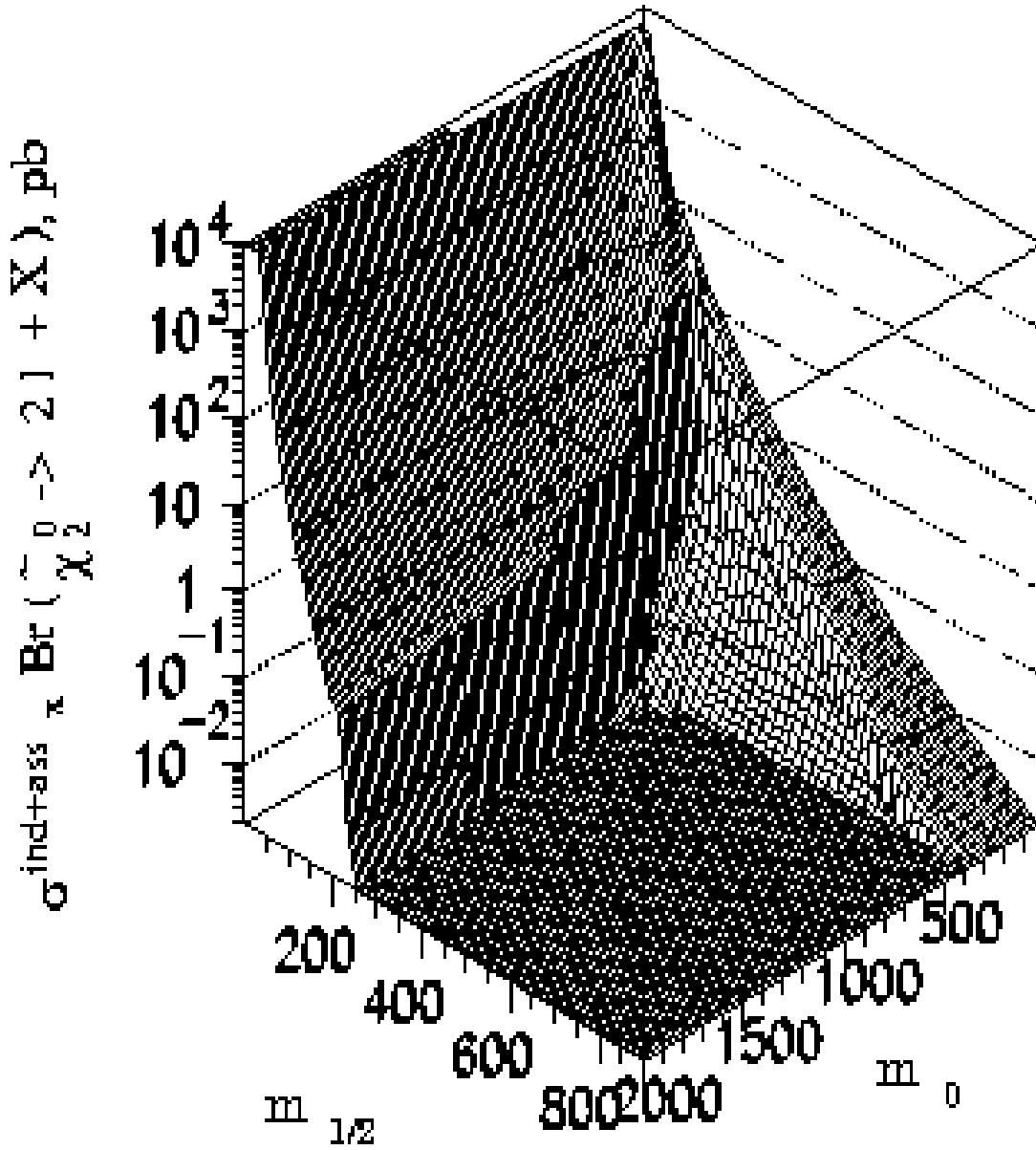


Figure 6: Sigma times branching ratios for indirect and associated production of $\tilde{\chi}_2^0$ followed by decays into leptons as a function of m_0 and $m_{1/2}$.

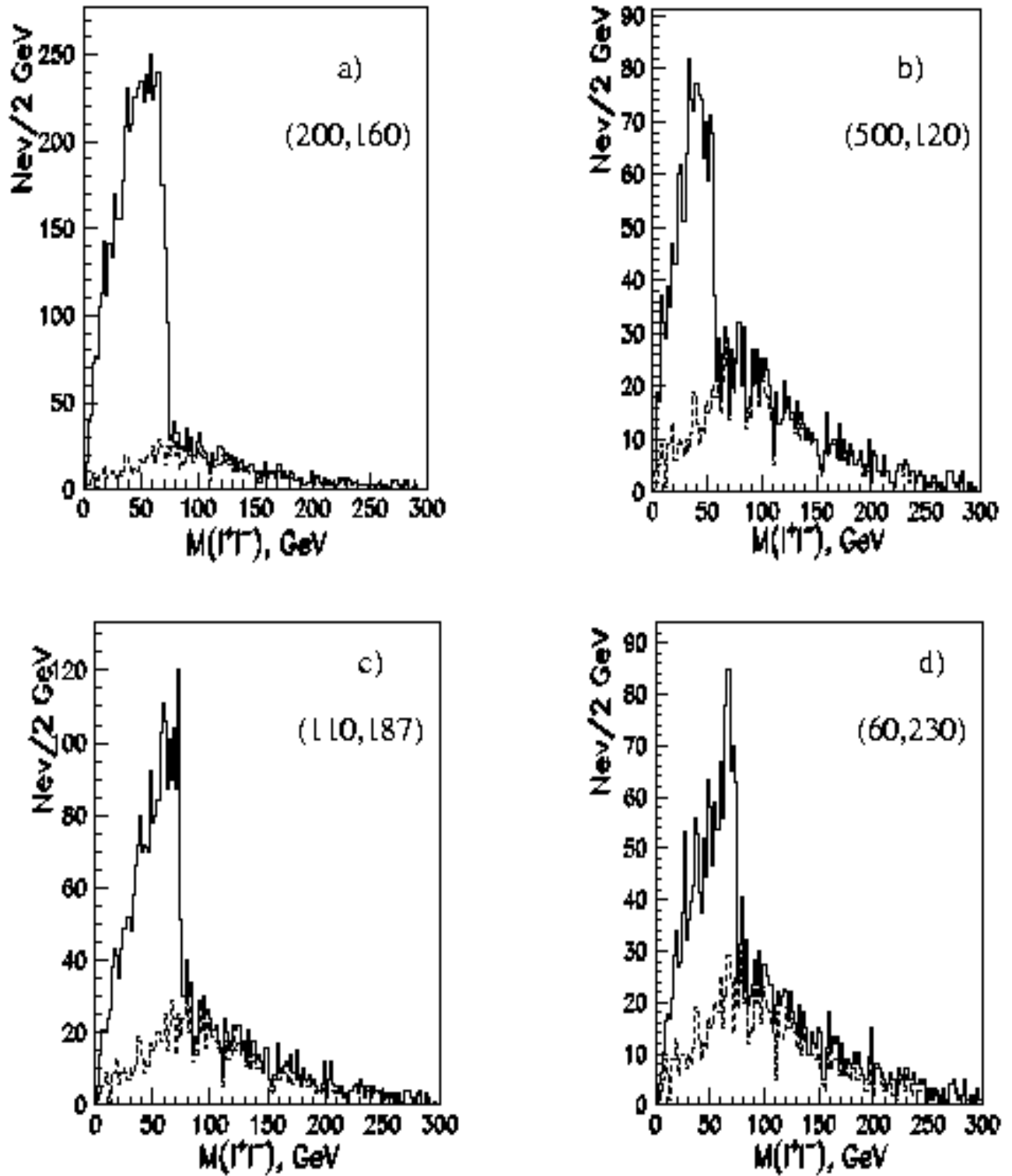


Figure 7: Invariant mass distribution of two same-flavour, opposite-sign leptons at various $(m_0, m_{1/2})$ points from domain I, II and III for $L_{int} = 10^3 \text{ pb}^{-1}$. SM background is also shown (dashed line).

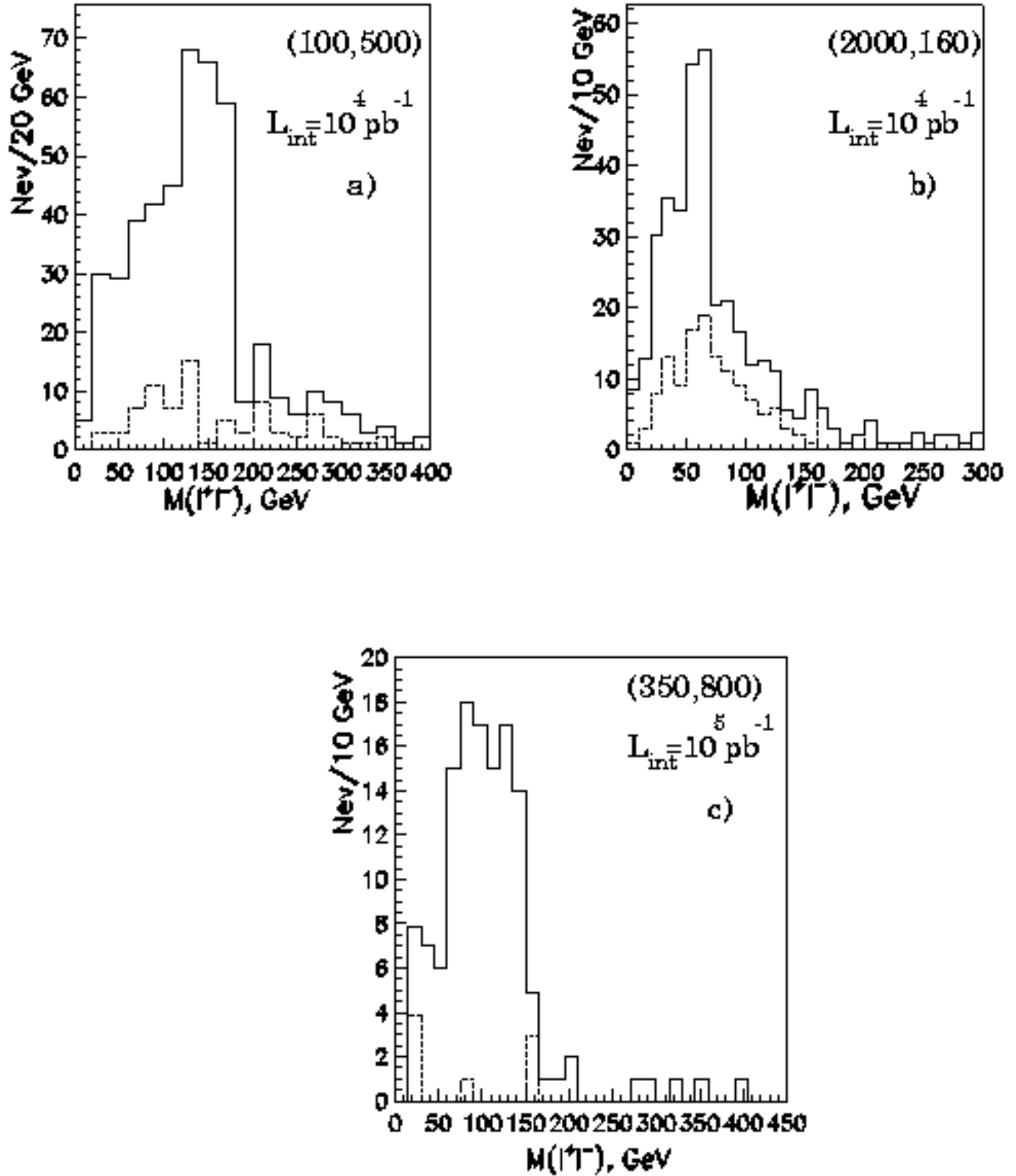


Figure 8: Invariant mass distribution of two same-flavour, opposite-sign leptons at $(m_0, m_{1/2})$ points from domain I, II and III close to the experimental reach at corresponding luminosities $L_{int} = 10^4 \text{ pb}^{-1}$ and 10^5 pb^{-1} . SM background is also shown (dashed line).

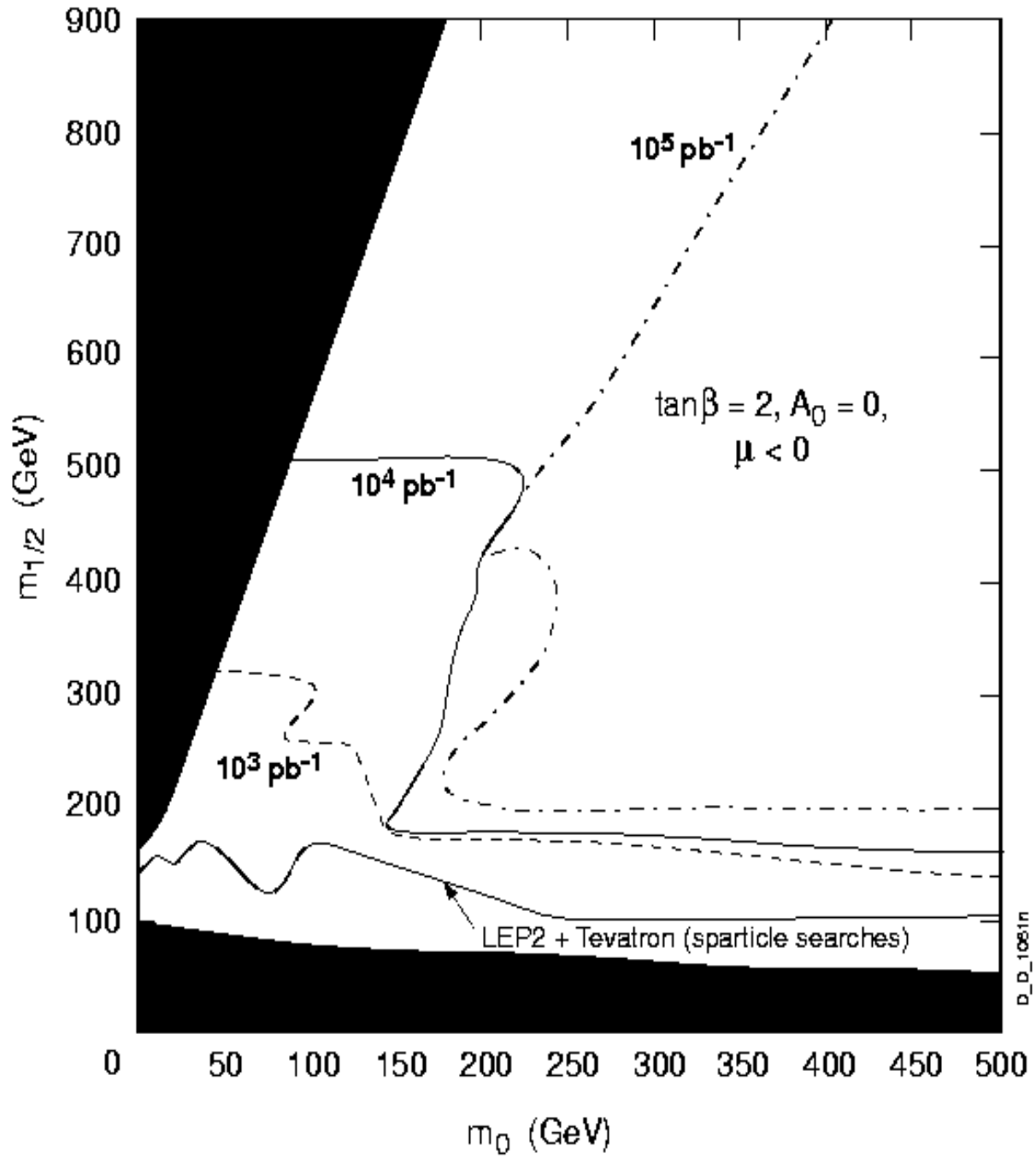


Figure 9: Observability of edges in invariant dilepton mass distribution with luminosities 10^3 pb^{-1} (dashed line), 10^4 pb^{-1} (solid line) and 10^5 pb^{-1} (dashed-dotted line). Also shown are the explorable domain in sparticle searches at LEP2 (300 pb^{-1}) and the Tevatron (1 fb^{-1}), theoretically and experimentally excluded regions [19].

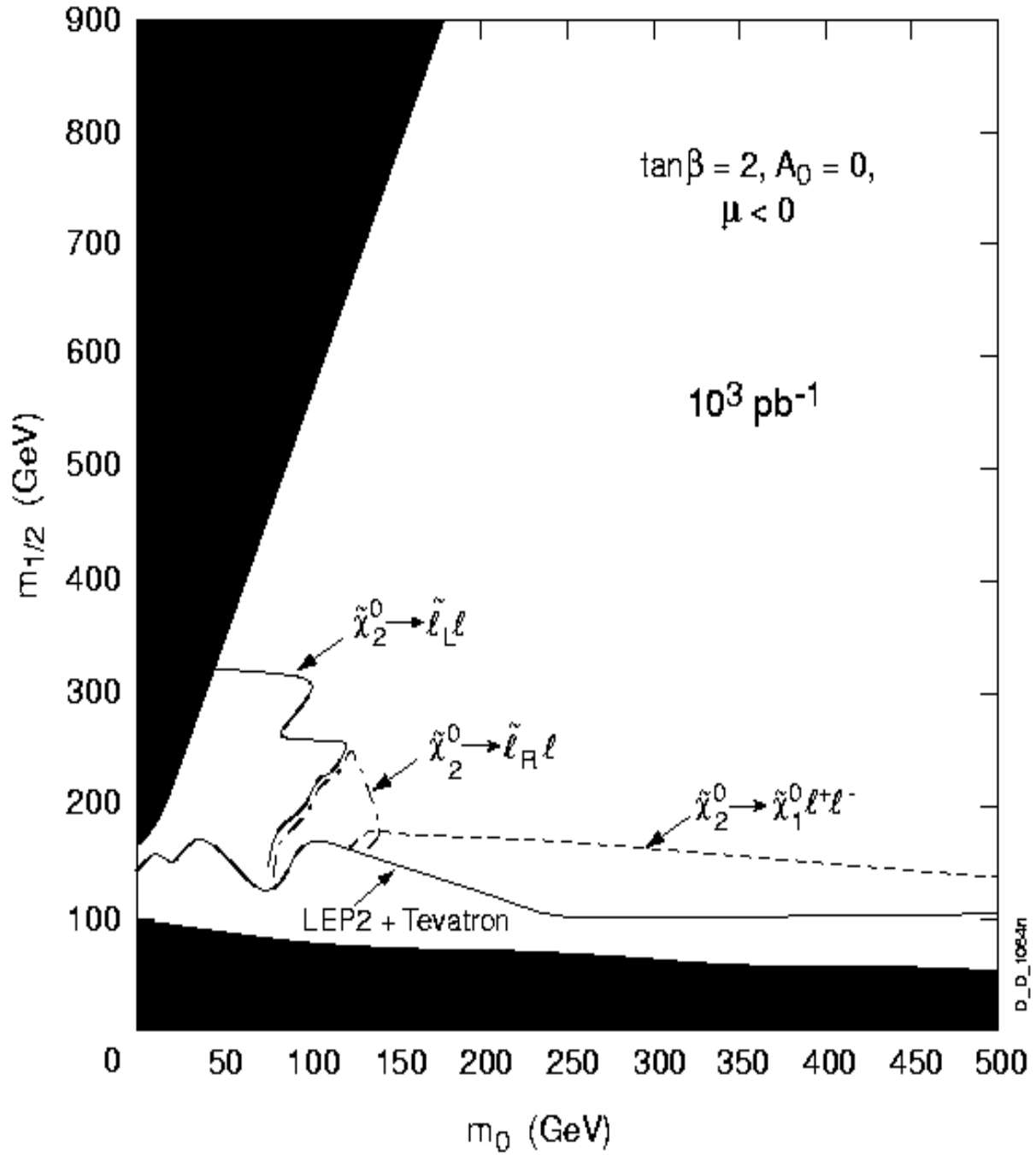


Figure 10: Domains where the observed edge in the M_{l+l^-} distribution is due to the decays $\tilde{\chi}_2^0 \rightarrow \tilde{l}_L^\pm l^\mp \rightarrow \tilde{\chi}_1^0 l^+ l^-$ (solid line), $\tilde{\chi}_2^0 \rightarrow \tilde{l}_R^\pm l^\mp \rightarrow \tilde{\chi}_1^0 l^+ l^-$ (dashed-dotted line), $\tilde{\chi}_2^0 \rightarrow \tilde{\chi}_1^0 l^+ l^-$ (dashed line), $L_{int} = 10^3 \text{ pb}^{-1}$.

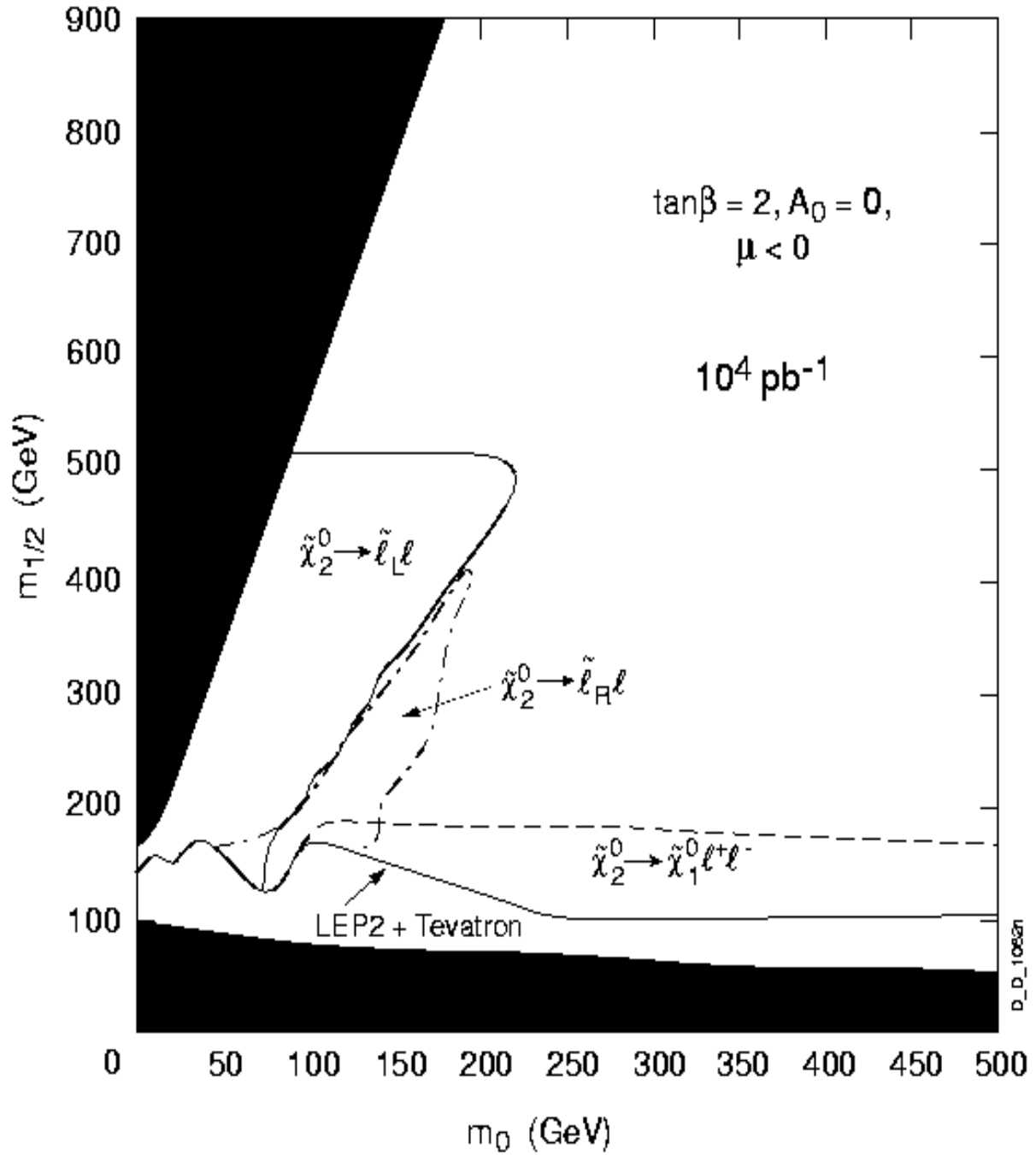


Figure 11: Domains where the observed edge in the M_{l+l^-} distribution is due to the decays $\tilde{\chi}_2^0 \rightarrow \tilde{l}_L^\pm l^\mp \rightarrow \tilde{\chi}_1^0 l^+ l^-$ (solid line), $\tilde{\chi}_2^0 \rightarrow \tilde{l}_R^\pm l^\mp \rightarrow \tilde{\chi}_1^0 l^+ l^-$ (dashed-dotted line), $\tilde{\chi}_2^0 \rightarrow \tilde{\chi}_1^0 l^+ l^-$ (dashed line), $L_{int} = 10^4 \text{ pb}^{-1}$.

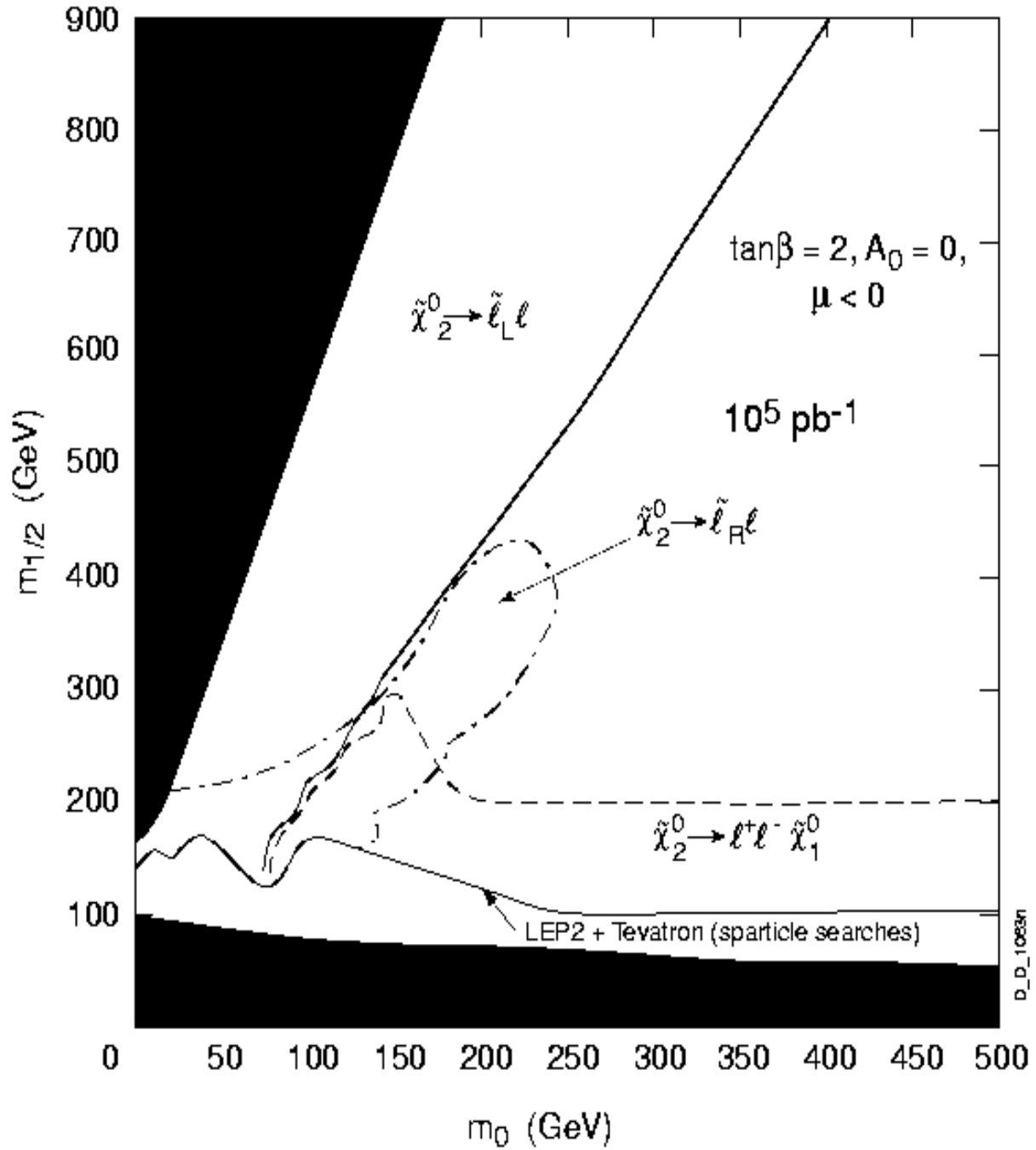


Figure 12: Domains where the observed edge in the M_{l+l^-} distribution is due to the decays $\tilde{\chi}_2^0 \rightarrow \tilde{l}_L^\pm l^\mp \rightarrow \tilde{\chi}_1^0 l^+ l^-$ (solid line), $\tilde{\chi}_2^0 \rightarrow \tilde{l}_R^\pm l^\mp \rightarrow \tilde{\chi}_1^0 l^+ l^-$ (dashed-dotted line), $\tilde{\chi}_2^0 \rightarrow \tilde{\chi}_1^0 l^+ l^-$ (dashed line), $L_{int} = 10^5 \text{ pb}^{-1}$.

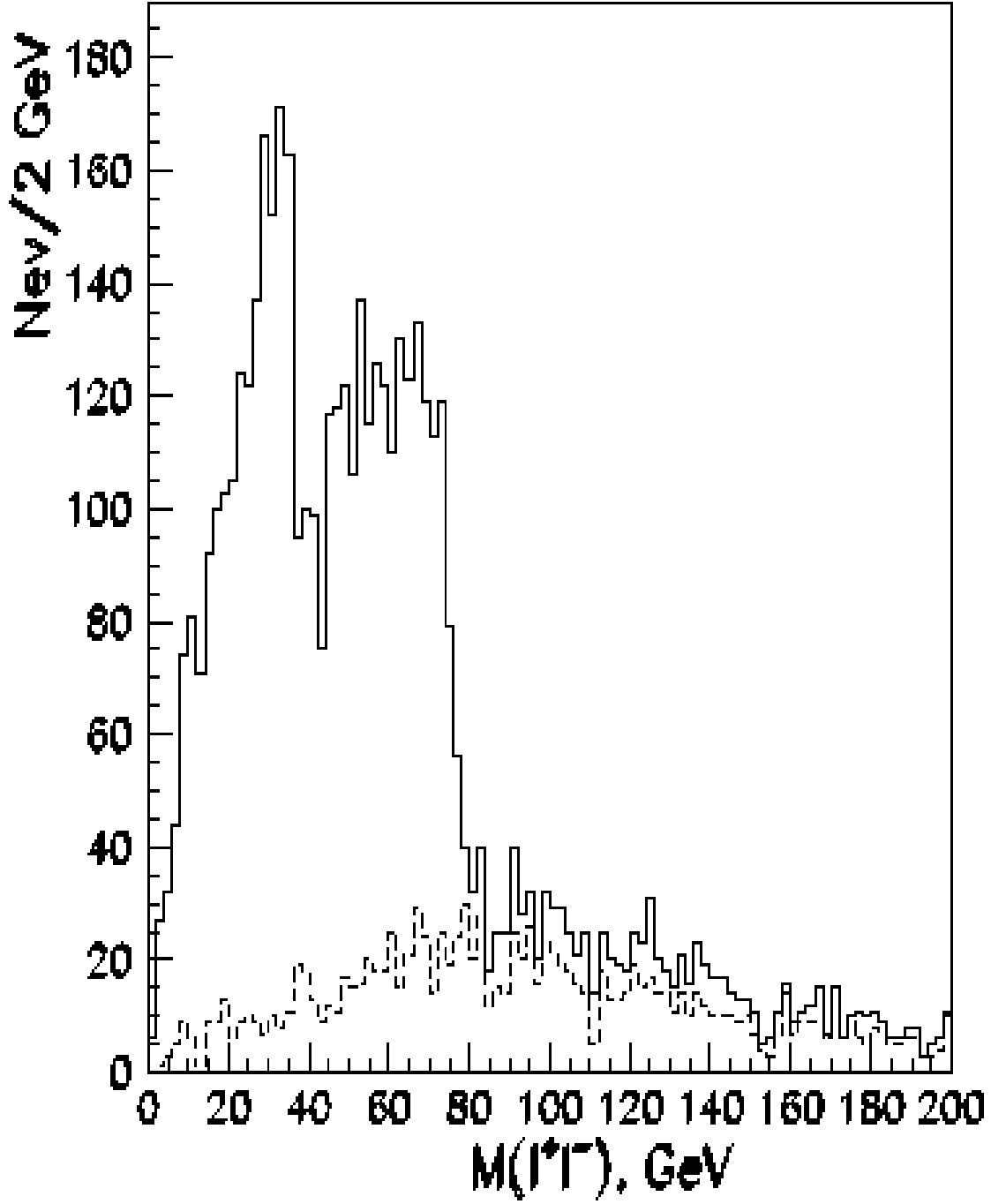


Figure 13: Invariant mass distribution of two same-flavour, opposite-sign leptons at the point $m_0 = 125$ GeV, $m_{1/2} = 170$ GeV, $L_{int} = 10^3$ pb $^{-1}$. SM background is also shown (dashed line). The edge at $M_{l+l^-} = 38$ GeV is due to the two-body $\tilde{\chi}_2^0 \rightarrow \tilde{l}_R^\pm l^\mp \rightarrow \tilde{\chi}_1^0 l^+ l^-$ decays and the edge at $M_{l+l^-} = 80$ GeV is due to the three-body $\tilde{\chi}_2^0 \rightarrow \tilde{\chi}_1^0 l^+ l^-$ decay.

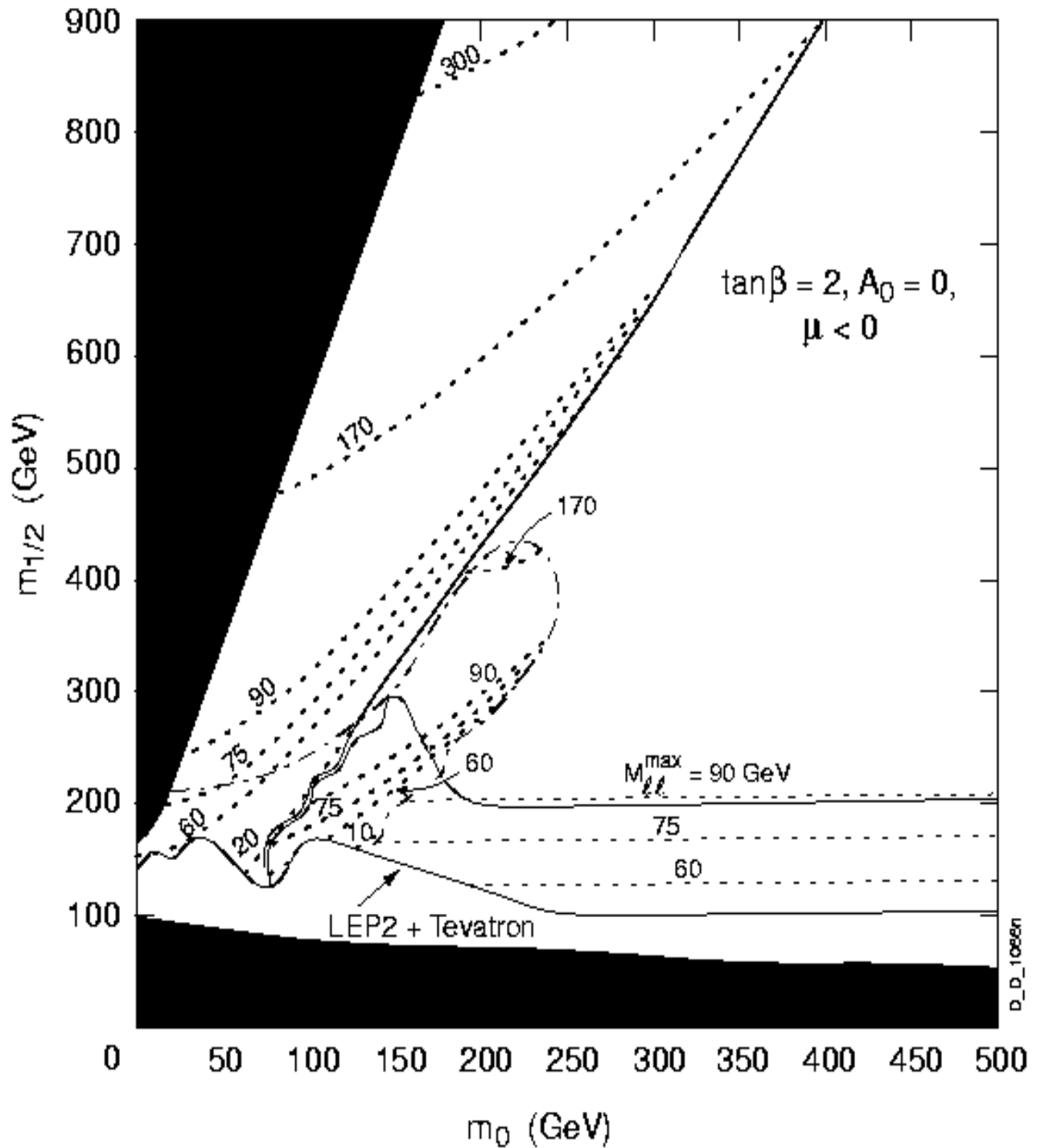


Figure 14: Contour lines of expected $M_{l+l^-}^{max}$ values (in GeV) in the invariant dilepton mass distribution corresponding to the three different $\tilde{\chi}_2^0$ decay modes in the region of the $(m_0, m_{1/2})$ parameter plane accessible with 10^5 pb^{-1} .

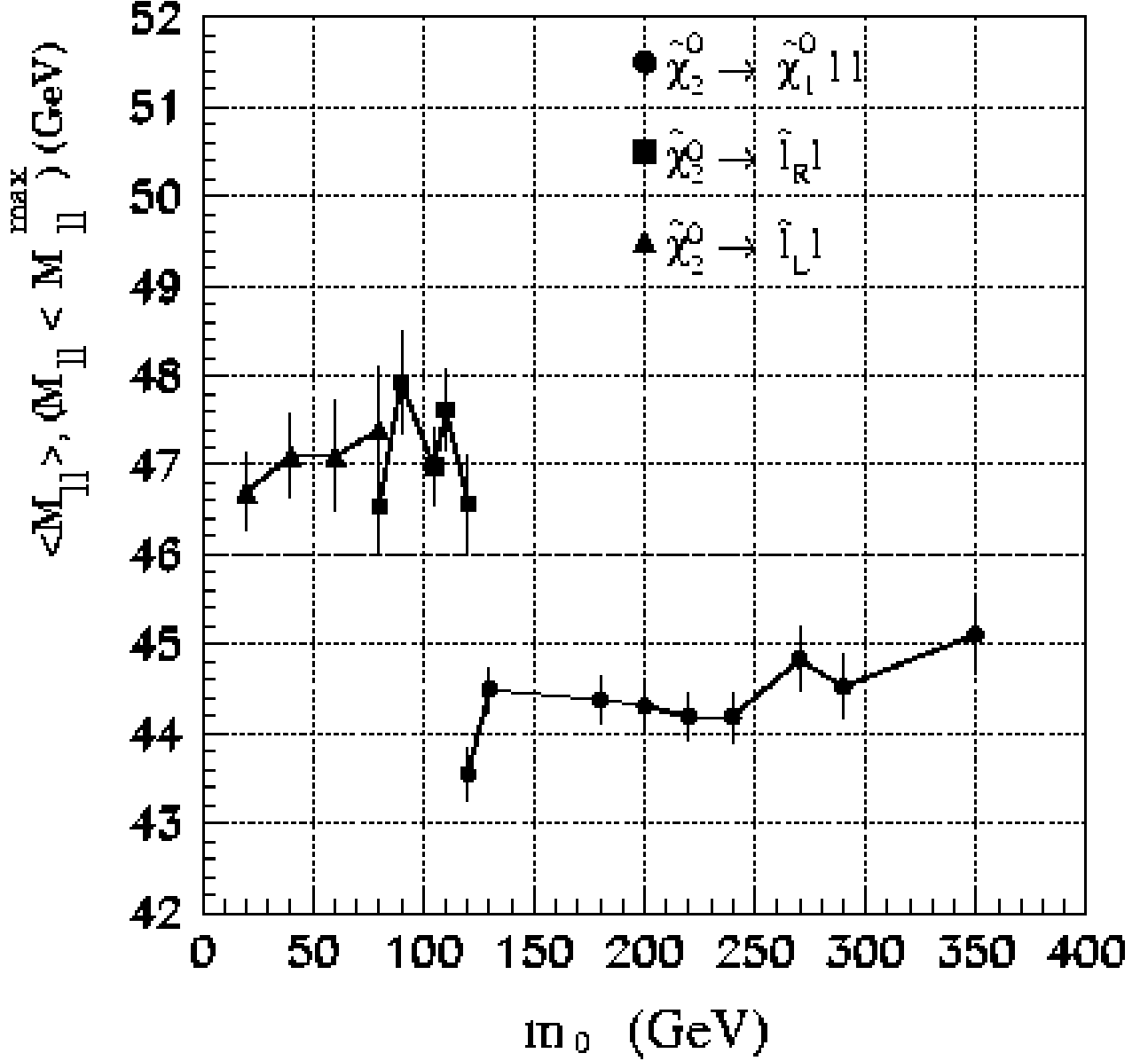


Figure 15: Average value of invariant dilepton mass, $M_{l+l^-} < M_{l+l^-}^{max}$ at $(m_0, m_{1/2})$ points with $M_{l+l^-}^{max} = 74 \pm 1$ GeV corresponding to the decays $\tilde{\chi}_2^0 \rightarrow \tilde{\chi}_1^0 l+l^-$, $\tilde{\chi}_2^0 \rightarrow \tilde{l}_L^\pm l^\mp \rightarrow \tilde{\chi}_1^0 l+l^-$ and $\tilde{\chi}_2^0 \rightarrow \tilde{l}_R^\pm l^\mp \rightarrow \tilde{\chi}_1^0 l+l^-$ as a function of m_0 ; $p_T^{l,2} > 15$ GeV, $E_T^{miss} > 100$ GeV, $L_{int} = 10^3$ pb $^{-1}$.

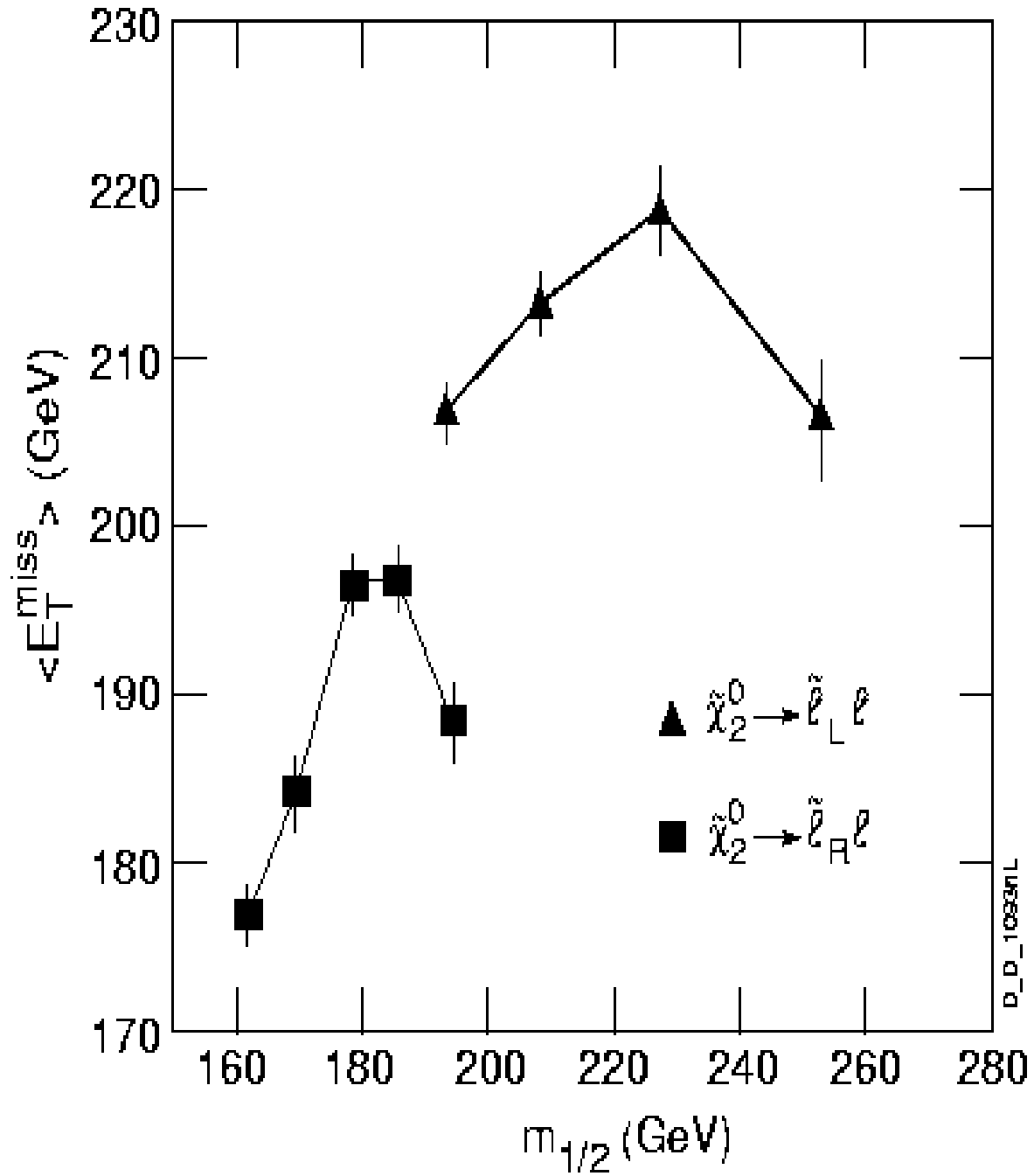


Figure 16: Average value of E_T^{miss} at $(m_0, m_{1/2})$ points with $M_{l^+l^-}^{max} = 74 \pm 1$ GeV corresponding to the decays $\tilde{\chi}_2^0 \rightarrow \tilde{l}_L^\pm l^\mp \rightarrow \tilde{\chi}_1^0 l^+ l^-$ and $\tilde{\chi}_2^0 \rightarrow \tilde{l}_R^\pm l^\mp \rightarrow \tilde{\chi}_1^0 l^+ l^-$ as a function of $m_{1/2}$, $L_{int} = 10^3$ pb $^{-1}$. Event selection criteria are: $p_T^{1,2} > 15$ GeV, $E_T^{miss} > 100$ GeV and $M_{l^+l^-} < M_{l^+l^-}^{max}$.

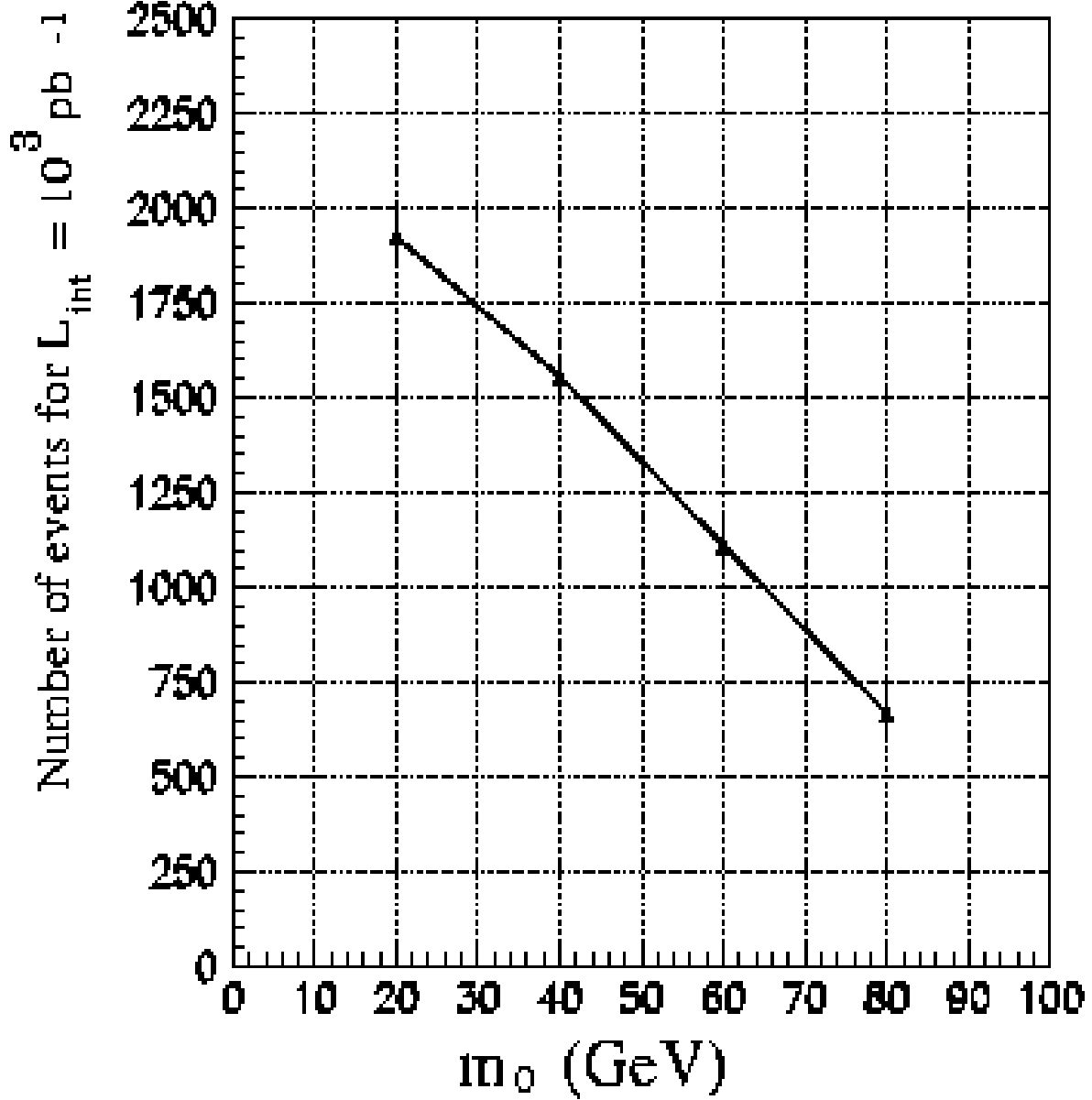


Figure 17: Expected $2l + E_T^{miss}$ event rate with $L_{int} = 10^3 \text{ pb}^{-1}$ along $M_{l+l^-}^{max} = 74 \pm 1 \text{ GeV}$ contour line in domain III ($\tilde{\chi}_2^0 \rightarrow \tilde{l}_L^\pm l^\mp \rightarrow \tilde{\chi}_1^0 l^+ l^-$) as a function of m_0 . Event selection criteria are: $p_T^{l_{1,2}} > 15 \text{ GeV}$, $E_T^{miss} > 130 \text{ GeV}$ and $M_{l+l^-} < M_{l+l^-}^{max}$ at corresponding points.

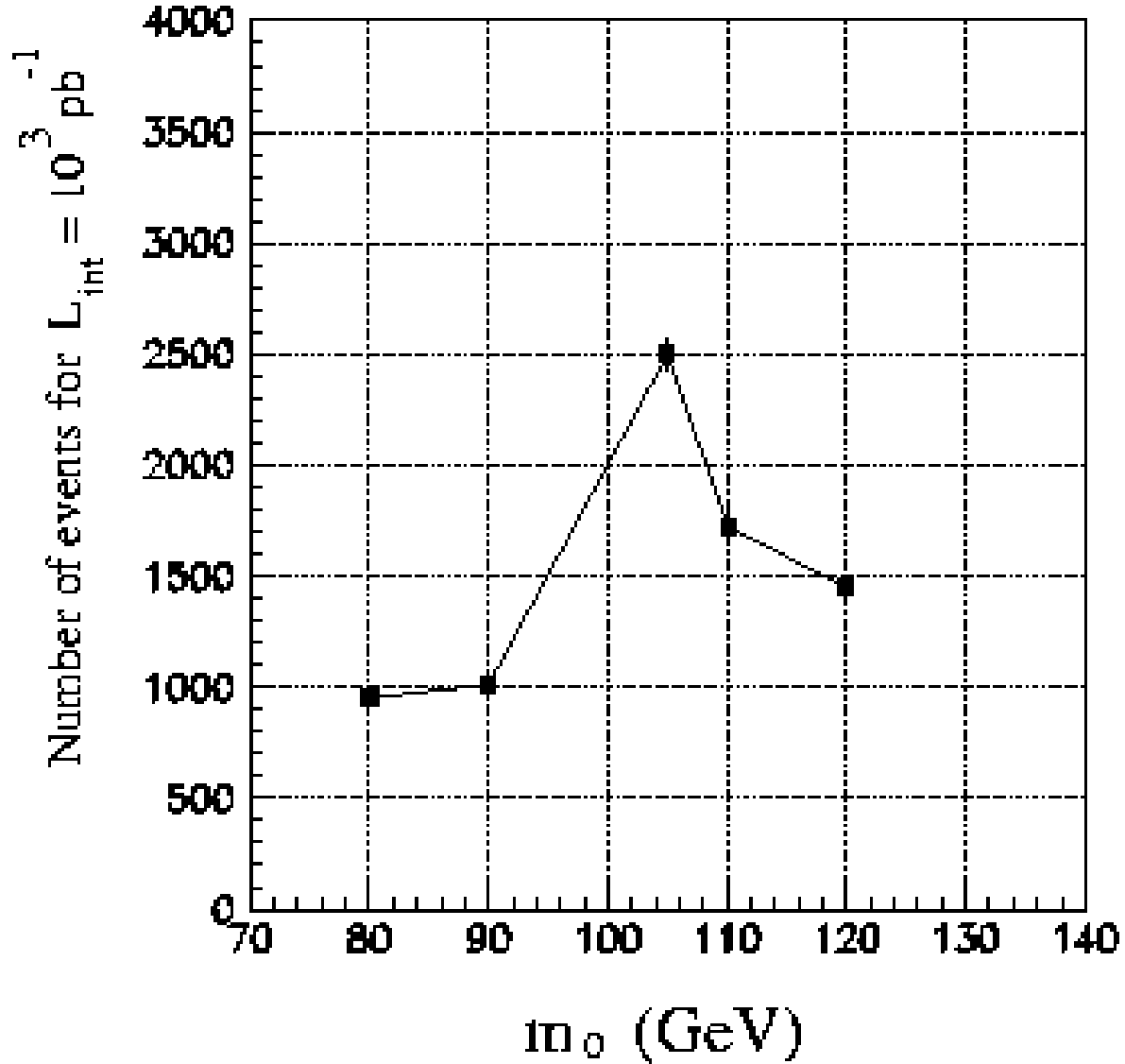


Figure 18: Expected $2l + E_T^{miss}$ event rate with $L_{int} = 10^3 \text{ pb}^{-1}$ along $M_{l+l-}^{max} = 74 \pm 1$ GeV contour line in domain II ($\tilde{\chi}_2^0 \rightarrow \tilde{l}_R^\pm l^\mp \rightarrow \tilde{\chi}_1^0 l^+ l^-$) as a function of m_0 . Event selection criteria are: $p_T^{l_{1,2}} > 15$ GeV, $E_T^{miss} > 130$ GeV and $M_{l+l-} < M_{l+l-}^{max}$ at corresponding points.

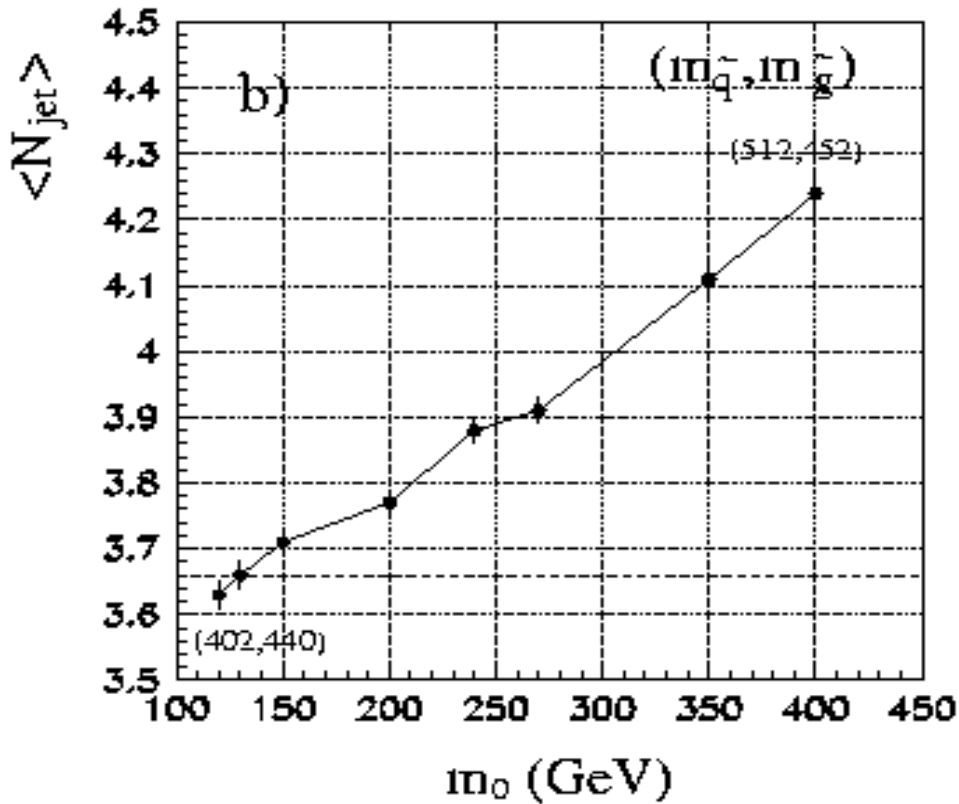
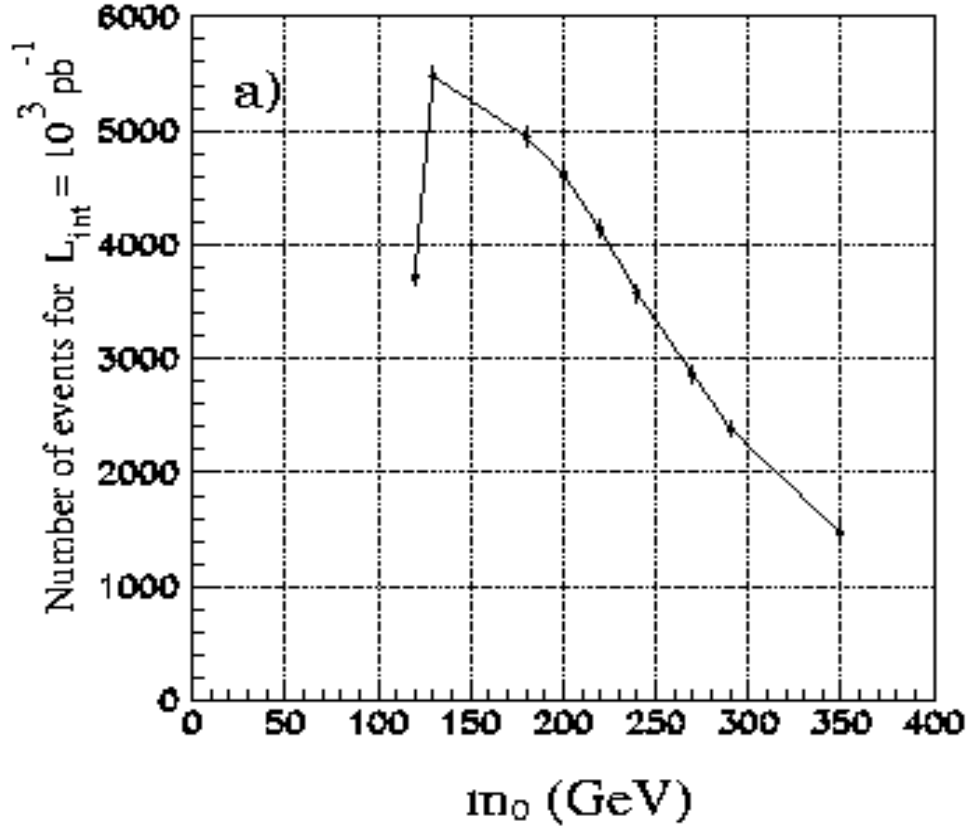


Figure 19: a) Expected $2l + E_T^{miss}$ event rate with $L_{int} = 10^3 \text{ pb}^{-1}$ along $M_{l+l^-}^{max} = 74 \pm 1$ GeV contour line in domain I ($\tilde{\chi}_2^0 \rightarrow \tilde{\chi}_1^0 l^+ l^-$) as a function of m_0 . Event selection criteria are: $p_T^{l_{1,2}} > 15$ GeV, $E_T^{miss} > 130$ GeV and $M_{l+l^-} < M_{l+l^-}^{max}$ at corresponding points; b) Average number of jets ($E_T^{jet} > 30$ GeV, $|\eta_{jet}| < 3$) at investigated points from domain I. The numbers in parenthesis show the masses of squarks and gluinos (in GeV) at corresponding points.